Article

Cell Reports

Mesenchymal-epithelial interaction regulates gastrointestinal tract development in mouse embryos

Graphical abstract

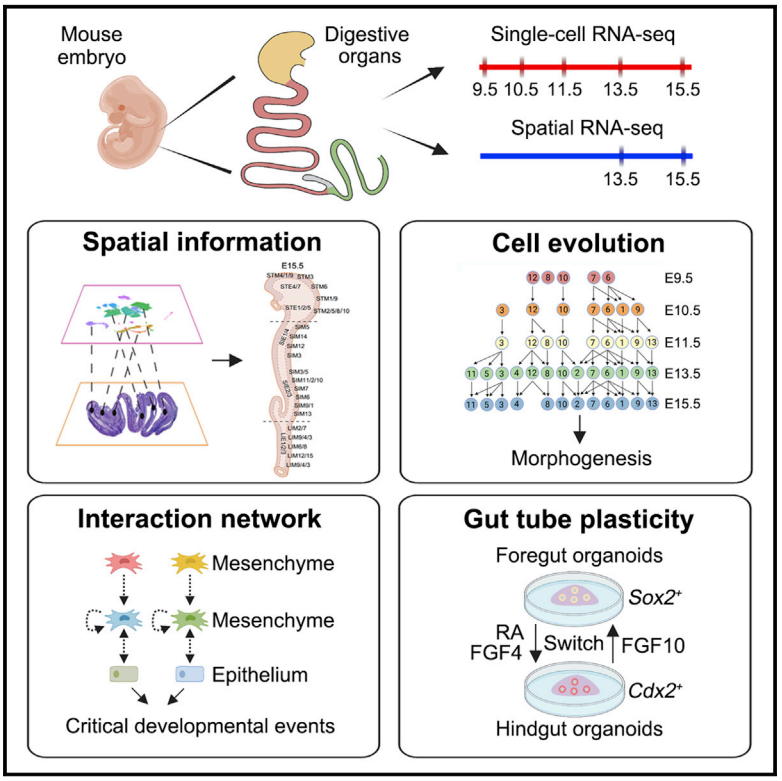

Highlights

- RNA-seq profiling reveals a dynamic cell atlas during early GI tract development
- Epithelial and mesenchymal regionalization can be detected at E9.5
- Mesenchymal-epithelial interactions regulate developmental events of the GI tract
- Gut tube cells possess plasticity and cell fate can be switched by regional factors

Authors

Lianzheng Zhao, Wanlu Song, Ye-Guang Chen

Correspondence

ygchen@tsinghua.edu.cn

In brief

Based on single-cell and spatial RNA sequencing, Zhao et al. depict a comprehensive transcriptomic landscape of the developing mouse stomach and small and large intestine during E9.5–E15.5. This landscape reveals a dynamic cell atlas, uncovers the early regionalization process, and reveals mesenchymal-epithelial interactions regulating critical developmental events and cell fate determination.

Zhao et al., 2022, Cell Reports *40*, 111053
July 12, 2022
https://doi.org/10.1016/j.celrep.2022.111053

CellPress

Cell Reports

CellPress
OPEN ACCESS

Article

Mesenchymal-epithelial interaction regulates gastrointestinal tract development in mouse embryos

Lianzheng Zhao,[1,3] Wanlu Song,[1,3] and Ye-Guang Chen[1,2,4,*]

[1]The State Key Laboratory of Membrane Biology, Tsinghua-Peking Center for Life Sciences, School of Life Sciences, Tsinghua University, Beijing 100084, China

[2]Guangzhou Laboratory, Guangzhou, China

[3]These authors contributed equally

[4]Lead contact

*Correspondence: ygchen@tsinghua.edu.cn

https://doi.org/10.1016/j.celrep.2022.111053

SUMMARY

After gut tube patterning in early embryos, the cellular and molecular changes of developing stomach and intestine remain largely unknown. Here, combining single-cell RNA sequencing and spatial RNA sequencing, we construct a spatiotemporal transcriptomic landscape of the mouse stomach and intestine during embryonic days E9.5–E15.5. Several subpopulations are identified, including *Lox*$^+$ stomach mesenchyme, *Aldh1a3*$^+$ small-intestinal mesenchyme, and *Adamdec1*$^+$ large-intestinal mesenchyme. The regionalization and heterogeneity of both the epithelium and the mesenchyme can be traced back to E9.5. The spatiotemporal distributions of cell clusters and the mesenchymal-epithelial interaction analysis indicate that a coordinated development of the epithelium and mesenchyme contribute to the stomach regionalization, intestine segmentation, and villus formation. Using the gut tube-derived organoids, we find that the cell fate of the foregut and hindgut can be switched by the regional niche factors, including fibroblast growth factors (FGFs) and retinoic acid (RA). This work lays a foundation for further dissection of the mechanisms governing this process.

INTRODUCTION

After gastrulation, the endoderm gives rise to the gut tube epithelium surrounded by the mesoderm-derived mesenchyme at around embryonic day (E) 8.0 in mice (Spence et al., 2011; Zorn and Wells, 2009). Then the gut tube is patterned and specified into foregut, midgut, and hindgut regions at E8.5 (Han et al., 2020). E9.5–E15.5 is a critical time period for gastrointestinal (GI) tract morphogenesis: the stomach bud appears at E9.5 (Spence et al., 2011; Zorn and Wells, 2009), the stomach regionalization at E13.5 (Kim and Shivdasani, 2016), distinction of the small intestine from the large intestine at E11.5 (Nichol and Saijoh, 2011), and villus formation at E14.5 (Chin et al., 2017; Shyer et al., 2015; Walton et al., 2012). Gut tube regionalization and maturation are mainly modulated by the instructive signals from adjacent mesoderm (Kim and Shivdasani, 2016; Le Guen et al., 2015; Loe et al., 2021; McCracken and Wells, 2017; Spence et al., 2011). However, the interaction landscape between epithelium and mesenchyme during GI tract development remains largely unknown. Single-cell RNA sequencing (scRNA-seq) paves an unprecedented path to understanding the process of embryo development (Argelaguet et al., 2019; Briggs et al., 2018; Cao et al., 2019; Mohammed et al., 2017; Nowotschin et al., 2019; Peng et al., 2019; Pijuan-Sala et al., 2019). scRNA-seq has revealed the role of cell interaction networks in the mouse gut tube (Dong et al., 2018; Han et al., 2020; Sayols et al., 2020); however, some key time points and important segments have not been covered. The research on human embryos has not covered the key morphogenesis events of GI tract development (Gao et al., 2018; Holloway et al., 2021). Therefore, the transcriptomic profiling and interaction networks of the GI tract during the key morphogenesis events in mouse or human embryos remain to be depicted.

In this study, we establish a single-cell transcriptomic landscape of the developing mouse stomach and intestine during E9.5–E15.5. Using spatial RNA-seq, we charted cell evolution and distribution along embryo development. We found that epithelial regionalization and mesenchymal heterogeneity exist at E9.5. Our study also provides comprehensive information regarding the dynamics of signaling networks between epithelial and mesenchymal subgroups that are associated with critical developmental events. Finally, we establish the organoids derived from the foregut and hindgut. Based on the analysis of the mesenchymal-epithelial interactions, we show that the cell fates of the foregut and hindgut can be switched in the organoids upon ligand stimulation, highlighting the importance of niche signaling in the development of the digestive tract.

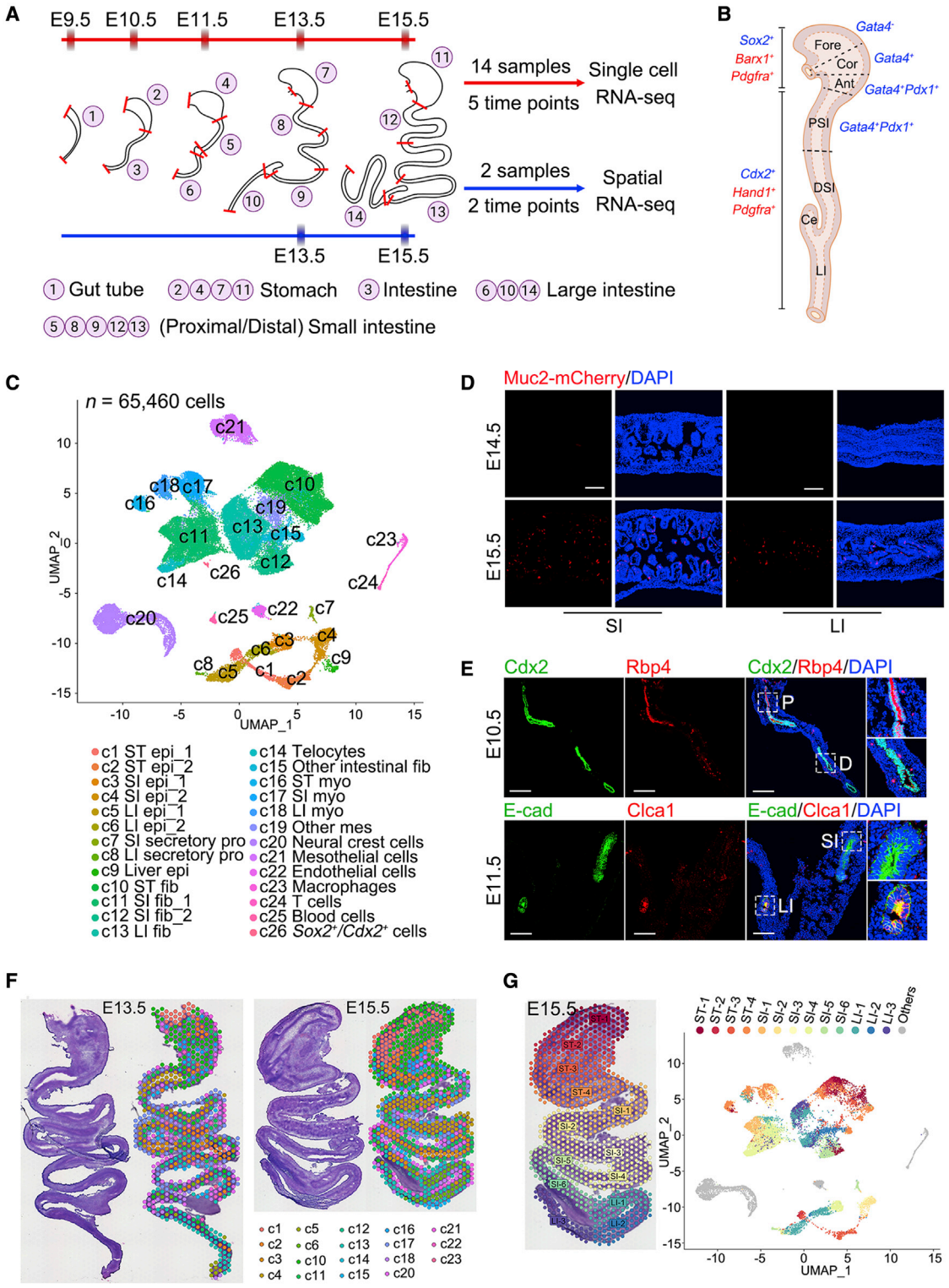

Figure 1. Single-cell and spatial transcriptional atlases of developing mouse stomach and intestine

(A) Fourteen samples from five time points were collected for scRNA-seq and two samples at E13.5 and E15.5 for spatial RNA-seq.

(B) Known markers of different regions used in this study. Epithelial and mesenchymal markers are depicted in blue and red, respectively. Fore, forestomach; Cor, corpus; Ant, antrum; PSI, proximal small intestine; DSI, distal small intestine; Ce, cecum; LI, large intestine.

(legend continued on next page)

RESULTS

Gene expression profiles of developing mouse stomach and intestine at single-cell resolution

To scrutinize the developmental process of the mouse stomach and intestine at early stages, we carried out single-cell transcriptome analyses of 14 individual samples covering five time points from E9.5 to E15.5 in mouse embryos using the 10× Chromium platform (Figure 1A). A total of 65,460 cells with an average expression of 4,597 genes per cell passed the quality control (Figure S1A). Cells could be classified into 26 groups (Figures 1B, 1C, S1B, and S1C and Table S1). Two stomach epithelium clusters (c1 and c2) were distinguished by *Gata4*, a hindstomach-specific marker (Willet and Mills, 2016). We observed two distinct small-intestinal epithelium clusters (c3 and c4), corresponding to the distal (epithelium 1) and proximal (epithelium 2) part, respectively (Figures 1B, 1C, and S1C), and large-intestinal epithelial cells also consisted of two clusters (c5 and c6) (Figures 1C and S1C). Within the secretory progenitors (*Tff3*$^+$) of the small intestine (c7) and large intestine (c8), some cells expressed the goblet marker *Muc2* (Figures 1C and S1C), which was confirmed in the E15.5 embryos of Muc2 reporter mice (Figure 1D). A small fraction of liver epithelium (c9) was also observed (Figures 1C and S1C).

The largest portion of the cells belonged to mesenchymal cells, including fibroblasts (*Pdgfra*$^+$) and myofibroblasts/myocytes (*Myh11*$^+$/*Des*$^+$) (c10–c19), and their distinct distributions in uniform manifold approximation and projection (UMAP) reflect remarkable differences between the stomach (c10), the proximal small intestine (c11), the distal small intestine (c12), and the large intestine (c13) (Figures 1C and S1C). Intriguingly, telocytes (c14) were found in the proximal small intestine as early as E13.5 (Figures 1C, S1B, and S1C), the time point before villus emergence, implying that niche cells may play crucial roles during epithelium morphogenesis. The cell clustering of individual samples was also profiled (Figures S1D–S1F).

The regionalized information of early gut tube was largely unknown and our scRNA-seq data revealed regionalized markers. For instance, *Cym*, *Bace2*, and *Abi3bp* were specifically expressed in the E11.5 stomach epithelium, while *Six2* was specific in the E9.5–E11.5 stomach mesenchyme (Table S2). In the small-intestinal epithelium, *Serpina1e* appeared during E9.5–E10.5, *Hopx* appeared at E11.5, and *Rbp4* appeared during E9.5–E11.5. *Tdo2*, *Lum*, and *Gpr50* were specifically expressed in the small-intestinal mesenchyme during E9.5–E10.5 (Table S2). As for the large intestine, *Ntm* and *Fabp1* were found in the E9.5–E11.5 epithelium, and *Clca1* appeared at E10.5–E11.5. In addition to some *Hox* genes, *Sst* and *Pdlim5* appeared in the E10.5–E11.5 large-intestinal mesenchyme (Table S2). The expression of *Rbp4* in the small-intestinal epithelium and *Clca1* in the large-intestinal epithelium was validated by immunofluorescence (Figure 1E).

Spatial distribution of cell clusters

To learn cell spatial distribution during the development of the GI tract, we conducted 10× Visium spatial RNA-seq of the stomach and intestine at E13.5 and E15.5 (Figure 1A, ~1,700 spots, ~3,500 genes/spot). Spatial cell clusters were predicted in combination with the scRNA-seq data. Most spots in E13.5 and E15.5 slides corresponded well to the known cell types (Figure 1F), and some genes were restricted in certain regions, such as *Sox2*$^+$ stomach epithelium and *Cdx2*$^+$ intestinal epithelium distributed close to the lumen, *Gata4*$^+$ epithelium in the proximal small intestine and hindstomach, and *Des*$^+$ myocytes in the outer region of the E15.5 GI tract (Figure S2A).

Next, to locate the regional distribution of the cell clusters along the GI tract, we manually partitioned the slides into different regions based on the organ morphology and cell position (inner epithelium and outer mesenchyme) and found that clusters in different spots were highly correlated with distinct regions (Figures S2B and S2C). For instance, the spots in the forestomach and hindstomach corresponded to c1 and c2, respectively, highlighting the consistency between the spatial RNA-seq and scRNA-seq datasets. Therefore, by aligning the regions of the E15.5 sample with the UMAP results, we obtained the spatial information of epithelial and mesenchymal cells (c1–c19) in UMAP (Figure 1G). Moreover, except for the known stomach mesenchymal marker *Barx1*, we identified other markers for different regions, including *Sulf1* and *Igf1* at the future cardia; *Nkx2-5* and *Agr2* at the future pylorus; *Krts*, *Pitx1*, and *Ly6d* in the E15.5 forestomach; *Prap1*, *Fabp1*, and *Cps1* in the E15.5 proximal small intestine; and *Hoxb13* and *Fxyd4* in the E13.5 terminal large intestine (Figures S2D and S2E).

Coordinated development of epithelium and mesenchyme

To delineate the GI tract developmental process, we extracted the epithelial and mesenchymal cells from our scRNA-seq dataset and reclustered the cells of each organ independently. Except for *Neurod1*$^+$ secretory progenitors in STE9, based on *Gata4* expression (Willet and Mills, 2016), stomach epithelial (STE) cells could be grouped into high (STE1/2/5), low (STE3/6), and negative subsets (STE4/7/8) (Figures 2A and S3A and Table S1), where high and negative subsets correspond to the

(C) UMAP visualization of 26 single-cell clusters (c1–c26) comprising 65,460 cells was integrated from 14 scRNA-seq samples. Cell clusters are annotated based on known marker genes. ST, stomach; SI, small intestine; LI, large intestine; epi, epithelium; mes, mesenchyme; fib, fibroblasts; myo, myofibroblasts/myocytes; pro, progenitors.

(D) Distribution of Muc2$^+$ goblet cells in the small and large intestine of E14.5 and E15.5, as indicated by Muc2-mCherry. Scale bars, 100 μm.

(E) Expression of Rbp4 and Clca1 in the intestine as revealed by immunofluorescence staining. Longitudinal sections of E10.5 and E11.5 digestive tracts were used (n = 3). Cdx2 marks the intestinal epithelium, and E-cad marks the epithelium. Scale bars, 200 μm. P, proximal; D, distal.

(F) Alignment of spatial RNA-seq spots with scRNA-seq clusters. H&E staining shows tissue structures used for spatial RNA-seq. All spots were annotated based on scRNA-seq clusters. Note that c7, c8, c9, and c19 were not detected in spatial RNA-seq.

(G) Spatial distribution of single cells in UMAP. The spots of the E15.5 sample were manually partitioned into 13 regions, and then single cells in UMAP were aligned to these regions. From proximal to distal, the stomach, small intestine, and large intestine were partitioned into four, six, and three regions, respectively. See also Figures S1 and S2 and Tables S1 and S2.

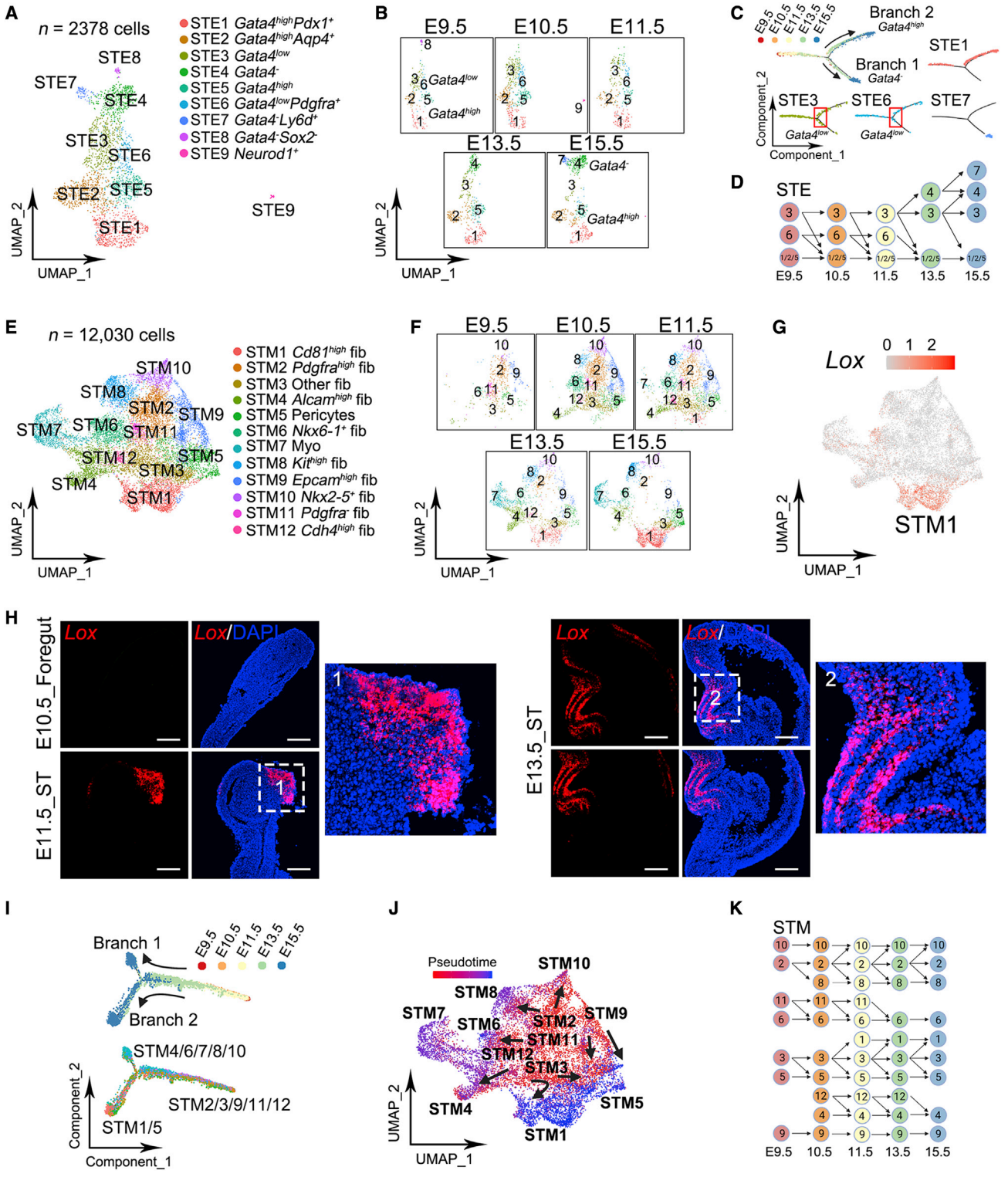

Figure 2. Cell evolution in the developing stomach

(A and B) UMAP visualization of stomach epithelial subsets (STE) (A) and their dynamic changes at different time points (B). Subsets are characterized by specific or highly expressed genes. The cluster number in (B) is related to (A).

(C) Trajectories of STE development. Results shown are based on developmental stage and separated subset. The red boxes indicate *Gata4*^{low} cells located at both the *Gata4*^{high} and the *Gata4*$^{-}$ branches.

(legend continued on next page)

hindstomach and forestomach epithelium (Willet and Mills, 2016), respectively. Notably, the forestomach epithelial STE4 and STE7 emerged at E13.5 and E15.5, respectively (Figure 2B). *Gata4* plays an essential role in stomach epithelium morphogenesis (DeLaForest et al., 2021; Jacobsen et al., 2005; Jacobsen et al., 2002). Trajectory analysis showed that *Gata4*^{low} cells moved toward the regionalized branches of *Gata4*$^{-}$ and *Gata4*^{high} (Figures 2C, S3B, and S3C) and almost diminished at E15.5 (Figure 2B), suggesting that they are in the intermediate state and play important roles in forestomach and hindstomach morphogenesis. The E9.5 STE could be divided into *Gata4*^{high} and *Gata4*^{low} groups (Figure 2B), implying that the progenitors for later regionalization are already present as early as E9.5, which is supported by the pattern of differentially expressed genes between these two groups at E9.5 (Figure S3D) and the presence of the *Pdx1*$^{+}$ antrum progenitors (STE1) at E9.5 (Figures 2A and S3A). Furthermore, compared with the *Gata4*^{high} group, the upregulated genes in the *Gata4*^{low} group are associated with epithelial proliferation and gland development (Figure S3E and Table S3). These results allowed us to reduce the cell evolution route (Figure 2D).

The stomach mesenchyme (STM) consisted of 12 subsets (Figures 2E and S3F and Table S1). Like the epithelium, the E9.5 STM already exhibited obvious heterogeneity (Figure 2F). STM1 emerged at E11.5, and its marker *Lox* was enriched in the proximal region and the boundary between the stomach and the esophagus (Figures 2G and 2H), implying that this subset may function in forestomach morphogenesis and organ segregation. Some genes also manifested region-specific distribution as indicated by E15.5 spatial sequencing (Figure S3G). For instance, *Ecm1* and *Prdm6* in STM4 were located at the forestomach, *Scx* and *Hand2os1* in STM8 at the hindstomach, *Pappa* and *Nkx6-1* in STM6 at the future cardia, and *Nkx2*-5 and *Col9a1* in STM10 at the future pylorus (Figure S3G). Of note, STM6 and STM10 expressed the esophagus and intestine mesenchymal markers *Nkx6-1* and *Hand1*, respectively (Figure S3F). The STM exhibited two distinct developmental branches, from early precursors (STM2/3/9/11/12) and targeting for branch 1 (STM4/6/7/8/10) and branch 2 (STM1/5) (Figures 2I and S3H). The trajectory analysis uncovered the cell evolution route (Figures 2J and 2K). Together, our data suggest that STE and STM coordinately develop from E9.5 to E15.5, with dramatic changes in cellular subsets.

The cells in the small-intestinal epithelium (SIE) could be clustered into three subsets, representing proximal *Fabp1*^{high} (SIE1) and *Pdx1*$^{+}$ (SIE4), distal *Osr2*$^{+}$ (SIE2/3), and a fraction of *Tff3*$^{+}$ secretory progenitor cells (SIE5) (Figures 3A and S4A and Table S1). The proximal and distal distinction already existed at E9.5 (Figure 3B). The functional difference between the proximal and the distal groups was reflected in the metabolic process (Figure S4B and Table S3). Trajectory analysis revealed two branches of development with one for secretory progenitors (Figures 3C, 3D, S4C, and S4D). Notably, the adult intestinal stem cell marker *Lgr5* appears in the distal epithelium (SIE2/3) at E9.5 and is highly enriched after E13.5 (Figure S4E), which was validated by *in situ* hybridization and the Lgr5 reporter mice showing its gradually increased expression from the proximal to the distal epithelium (Figures 3E and S4F). To explore the functions of *Lgr5*$^{+}$ cells in the developing small intestine, we traced the cell fate with *Lgr5-CreERT2;Rosa26-ZsGreen* mice. After tamoxifen induction at E11.5, only a small fraction of proximal epithelial cells could be traced at E15.5 (Figure 3F). These cells were randomly distributed at the villus tip or the region between adjacent villus, indicating that *Lgr5*$^{+}$ cells were not the stem cell progenitors at the early stage. Nevertheless, most distal epithelial cells were traced, as *Lgr5*$^{+}$ cells were enriched in the distal part. Together, these data indicate that *Lgr5*$^{+}$ cells may have different roles in the proximal and distal small intestine during development.

The small-intestinal mesenchyme (SIM) also displayed apparent divergence between the proximal (SIM3/5/8/9) and the distal (SIM1/2/4/7) groups (Figures 3G and S4G and Table S1). The cell heterogeneity existed as early as E9.5. E11.5 is the time point for cecum morphogenesis and small and large intestine segmentation (Nichol and Saijoh, 2011). SIM1/3/9/13 appeared at E10.5–E11.5, and SIM1/13 were close to the cecum, implicating their function in this process (Figure 3H). The cell number and appearance of SIM clusters were dynamic during E9.5–E15.5. For instance, the cell number of SIM3 was increased during the time. SIM11 clusters (*Foxl1*$^{+}$ telocytes), which are essential signaling resources in adult small intestine (Bahar Halpern et al., 2020; Shoshkes-Carmel et al., 2018), started to emerge at E13.5 (Figure 3H). The pseudotime analysis unveiled that SIM11 may be derived from SIM3, suggesting that SIM3 could be the origins of telocytes (Figures 3I–3K and S4H). This note was supported by the expression pattern of the SIM3 marker *Aldh1a3*, which existed at E11.5 before telocyte appearance and exhibited subepithelial distributions like those of telocytes at E13.5 (Figures 3L and 3M).

The large-intestinal epithelial cells (LIE) could also be clustered into different subsets, including the *Tff3*$^{+}$ secretory progenitor cells, which appeared at E15.5 (LIE6) (Figures 4A, 4B, and S5A and Table S1). The trajectory analysis indicated that these cells underwent three differentiation branches as indicated (Figures 4C, 4D, S5B, and S5C). LIE2 cells were more like small-intestinal epithelial cells, with the expression of *Osr2* and *Lgals2* (Figure S5A and Table S3). LIE4 cells, which were double

(D) Evolution map of STE development. Results are summarized from the trajectory analysis. Arrows indicate the possible evolution direction.
(E and F) UMAP visualization of stomach mesenchymal subsets (STM) (E) and their dynamic changes at different time points (F). Subsets are characterized by specific or highly expressed genes. fib, fibroblasts; myo, myofibroblasts/myocytes.
(G) UMAP visualization of *Lox* expression in STM.
(H) *In situ* hybridization of *Lox* expression in E10.5 foregut and E13.5 and E15.5 stomach. Longitudinal sections of fresh tissues were cut (n = 3). Scale bars, 200 μm.
(I) Trajectories of STM development. Results shown are based on developmental stages and mesenchymal subsets.
(J) UMAP visualization of STM based on pseudotime analysis. Arrows indicate possible development direction.
(K) Evolution map of STM development. Results are summarized from trajectory analysis. Arrows indicate the possible evolution direction. See also Figure S3 and Tables S1 and S3.

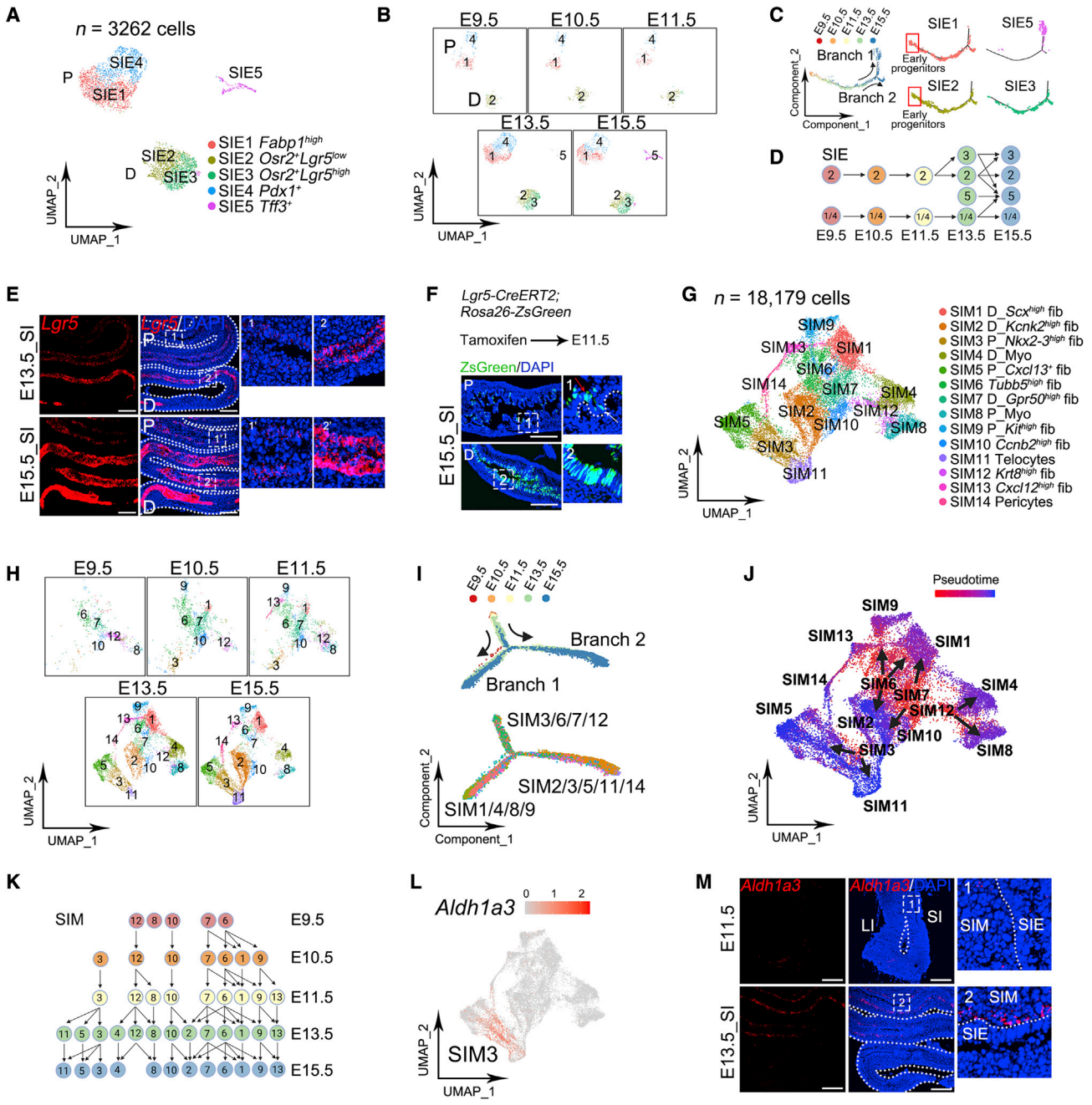

Figure 3. Proximal and distal cell divergence in the developing small intestine

(A and B) UMAP visualization of small-intestinal epithelial subsets (SIE) (A) and their dynamic changes at different time points (B). Subsets are characterized by specific or highly expressed genes. P, proximal; D, distal.

(C) Trajectories of SIE development. Results shown are based on developmental stages and separated subsets. The red boxes indicate early proximal and distal progenitors located at trajectory origins.

(D) Evolution map of SIE development. Results are summarized from trajectory analysis. Arrows indicate the possible evolution direction.

(E) *In situ* hybridization of *Lgr5* expression in E13.5 and E15.5 small intestine. Fresh small intestines (n = 3) were embedded in a zigzag pattern and longitudinal sections were cut. Scale bars, 200 μm. SI, small intestine.

(F) Lineage tracing of *Lgr5*$^{+}$ cells in small intestine after E11.5. *Lgr5-CreERT2;Rosa26-ZsGreen* mice were injected with tamoxifen once at E11.5. Then the small intestine in the E15.5 embryo was isolated and imaged. The white arrow indicates the positive cells located at the region between adjacent villi, while the red arrow indicates the positive cells at the villus tip. The dashed line outlines the villus structure. Scale bars, 200 μm.

(G and H) UMAP visualization of small-intestinal mesenchymal subsets (SIM) (G) and their dynamic changes at different time points (H). Subsets are characterized by specific or highly expressed genes. fib, fibroblasts; myo, myofibroblasts/myocytes.

(legend continued on next page)

positive for *Sox2* and *Cdx2*, the markers of foregut and hindgut, respectively, were restricted to only E9.5 (Figures 4B and S5A), which was confirmed by immunofluorescence (Figure 4E). LIE5 vanished after E11.5, which may be related to small and large intestine segmentation (Figure 4B). LIE3, which came from LIE1/5 and appeared at E13.5 (Figures 4B and 4D), was located at the terminal large intestine and expressed *Fxyd4* and *Hoxb13* (Figure S2D).

The large-intestinal mesenchyme (LIM) also showed a high level of heterogeneity comprising 15 subsets (Figures 4F and S5D and Table S1). At E9.5, LIM1 and LIM11 were the major subsets, which disappeared at E15.5 and E10.5, respectively (Figure 4G). Interestingly, the cell heterogeneity dramatically increased at E10.5 and E11.5, including LIM2/7 (Figure 4G). *Adamdec1*$^{+}$ LIM7 was distributed at the proximal large intestine in both E11.5 and E13.5 (Figures 4H and 4I). Similar to SIM1/13 in the small intestine, these dynamic subsets may also participate in cecum morphogenesis and small and large intestine segmentation. The trajectory analysis showed that there were two main origins for LIM subsets, LIM11 and LIM1, with the former giving rise first to LIM2/10/14 and finally to LIM7/15, and the latter first to LIM8/9/13 and finally to LIM3/4/6 (Figures 4J–4L and S5E).

Dynamic mesenchymal-epithelial interactions regulate critical developmental events in the stomach and intestine

To uncover the molecular connection between the epithelium and the mesenchyme, we analyzed the possible signaling interactions. The expression of ligands and receptors at E9.5–E11.5 showed apparent differences between the epithelium and the mesenchyme along time and in different organs (Figure S6A). Considering that the interactions between epithelial and mesenchymal subsets were complicated, we focused on the interactions that drive critical developmental events of these three organs. For the stomach, we analyzed the events of forestomach and antrum specification. The above trajectory analyses indicated that *Gata4*^{low} epithelial cells (STE3/6) might be involved in the morphogenesis of the forestomach (*Gata4*$^{-}$, STE4/7) (Figures 2C, 2D, and S3B), so we analyzed the signals received by STE3/6. STM1 could influence STE3/6 through NRG (neuregulin) and BMP signaling. Hh, fibroblast growth factor (FGF), and growth differentiation factor (GDF) signaling might be involved in autocrine regulation of STE3/6 evolution (Figure 5A and Table S4). STM1 appeared at E11.5 (Figure 2F), the time before STE4/7 emergence, implying its importance in forestomach morphogenesis. This subset was derived from STM3 (Figures 2I–2K), which received signals from other STMs, STEs, and itself. These signals might take part in the generation of STM1 from STM3 and subsequent forestomach morphogenesis (Figure 5A and Table S4). For the antrum specification, the formation of progenitors (*Pdx1*$^{+}$ STE1) might be regulated by multiple mesenchymal-derived signals, such as CXCL, NRG, and pleiotrophin (PTN), and autocrine BMP, GDF, FGF, and Hh (Figure 5B and Table S4). Therefore, these signals may function in antrum morphogenesis at later stages.

Next we scrutinized the key developmental events in the small intestine, including proximal and distal divergence and villus formation. Mesenchymal-epithelial interactions could contribute to the proximal and distal divergence and thus lay a foundation for the segmentation of the duodenum, jejunum, and ileum. The different signals received by proximal (SIE1/4) and distal (SIE2) epithelium might function in the proximal and distal divergence. Mesenchyme-derived NRG, CXCL, and energy homeostasis associated (ENHO) signaling might act on SIE1/4 in the proximal part, while transforming growth factor β (TGF-β), BMP, and Periostin signaling might function on SIE2 in the distal part (Figure 5C and Table S4). Autocrine signals were also detected, such as cell adhesion molecule (CADM), Notch, vitronectin (VTN), and Wnt in SIE2. For the villus formation, SIM11 was a subset at E13.5 derived from SIM3 at E11.5 and highly expressed *Pdgfra* (Figures 3H, 3K, and S4G), which could be the cells at the villus tip involved in villus formation (Karlsson et al., 2000; Walton et al., 2012). As shown in Figure 5D and Table S4, SIM3 could receive ncWnt, Periostin, and EDN (endothelin) signals from SIM6/8/12/13/14; Hh, platelet-derived growth factor (PDGF), and FGF signals from SIE1/4; and autocrine PDGFs, suggesting the role of combinatory signaling events in SIM3 to SIM11 evolution. In the large intestine, we focused on the segmentation between the small and the large intestine. The above data suggest that SIM1/13 and LIM2/7 may function in this event, during which SIM1/13 could be influenced by IGF, Kit, ncWnt, and Notch, while SIE2 might receive TGF-β, Wnt, and Periostin signals from SIM1/13 (Figure 5E and Table S4). LIM2/7 could receive FGF, PGDF, Hh, and PTN signals and influence LIE1/2 via BMP, ncWnt, Wnt, and PTN.

We then examined the expended or newly appeared mesenchymal subsets after E13.5, which may produce the signals to regulate the morphogenesis process and function in the late stage of the stomach and intestine. As possible interactions most likely occur between physically close epithelial and mesenchymal subsets, we analyzed their spatial distributions based on scRNA-seq and spatial RNA-seq at E15.5. As shown in Figures 5F and 5G, most mesenchymal subsets exhibited a regional distribution, such as STM1 in the proximal stomach, SIM3 in the proximal small intestine, and LIM7 in the proximal large intestine as described above. The increased STM1 in E13.5 could promote forestomach (*Gata4*$^{-}$) morphogenesis by secreting TGF-β, BMP, ncWnt, and insulin-like growth factor (IGF) (Figure 5H and Table S4), consistent with the report that ncWnt functions in forestomach development (Matsuyama et al., 2009). SIM5 could be the resources of BMP, ncWnt, IGF, and Notch to modulate SIE1/4 in the proximal small intestine.

(I) Trajectories of SIM development. Results shown are based on developmental stages and mesenchymal subsets.
(J) UMAP visualization of SIM based on pseudotime analysis. Arrows indicate possible development direction.
(K) Evolution map of SIM development. Results are summarized from trajectory analysis. Arrows indicate the possible evolution direction.
(L) UMAP visualization of *Aldh1a3* expression in SIM.
(M) *In situ* hybridization of *Aldh1a3* expression in E11.5 and E13.5 small intestine. Longitudinal sections of fresh tissues were cut (n = 3). The dotted lines indicate the boundaries of SI, LI, SIM, and SIE. Scale bars, 200 μm. See also Figure S4 and Tables S1 and S3.

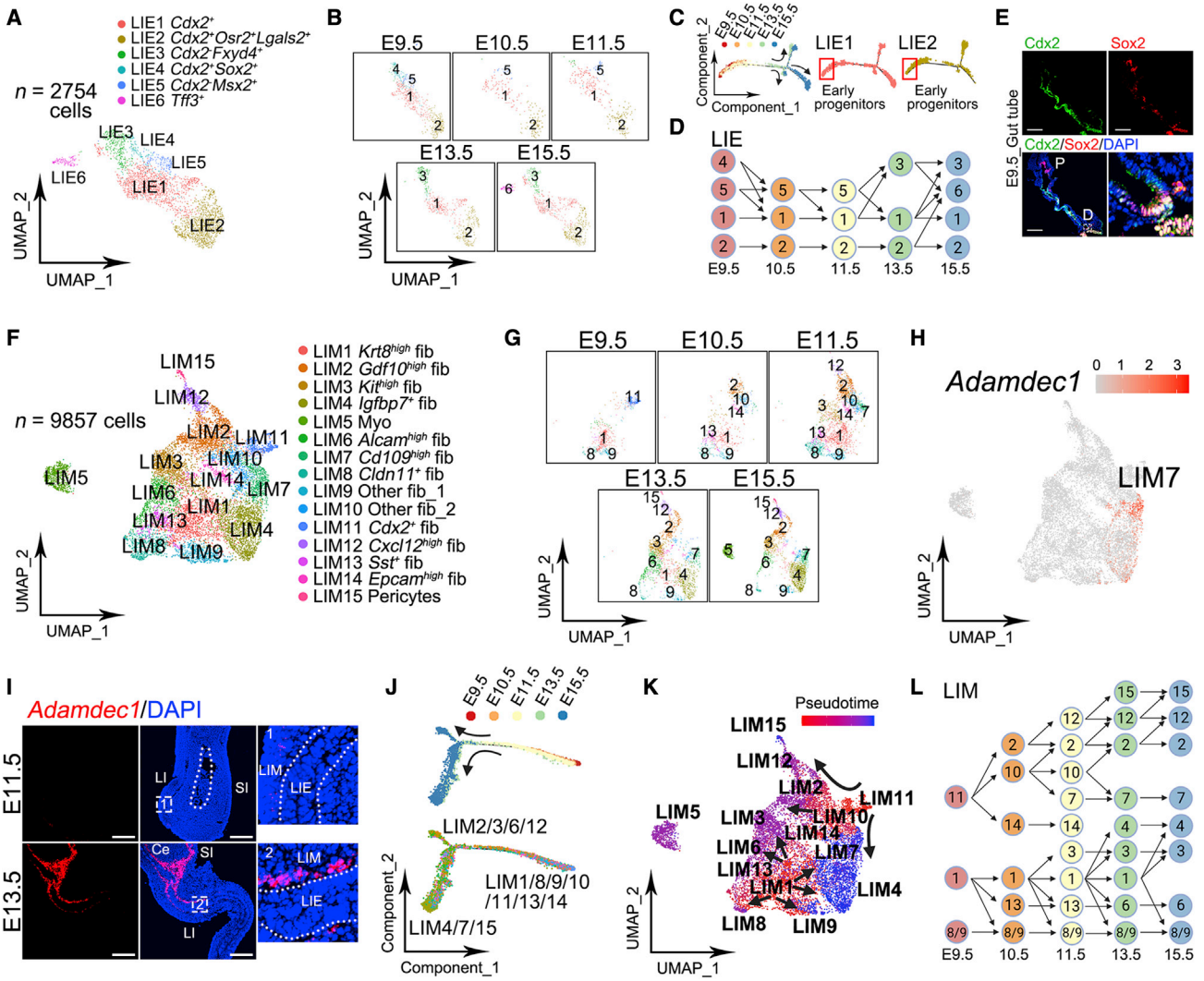

Figure 4. Cell heterogeneities during large intestine development

(A and B) UMAP visualization of large-intestinal epithelial subsets (LIE) (A) and their dynamic changes at different time points (B). Subsets were characterized by specific or highly expressed genes.

(C) Trajectories of LIE development. Results shown are based on developmental stages and separated subsets. The red boxes indicate early progenitors located at trajectory origins.

(D) Evolution map of LIE development. Results are summarized from trajectory analysis. Arrows indicate the possible evolution direction.

(E) Co-localization of Cdx2 and Sox2 at the terminal gut tube indicated by immunofluorescence staining. Longitudinal sections of E9.5 gut tube were used (n = 3). Scale bars, 200 μm. P, proximal; D, distal.

(F and G) UMAP visualization of large-intestinal mesenchymal subsets (LIM) (F) and their dynamic changes at different time points (G). Subsets are characterized by specific or highly expressed genes. fib, fibroblasts; myo, myofibroblasts/myocytes.

(H) UMAP visualization of *Adamdec1* expression in LIM.

(I) *In situ* hybridization of *Adamdec1* expression in E11.5 and E13.5 large intestine. Longitudinal sections of fresh tissues were cut (n = 3). The dotted lines indicate the boundaries of SI, LI, LIM, and LIE. Scale bars, 200 μm.

(J) Trajectories of LIM development. Results shown are based on developmental stages and mesenchymal subsets.

(K) UMAP visualization of LIM based on pseudotime analysis. Arrows indicate possible evolution direction.

(L) Evolution map of LIM development. Results are summarized from trajectory analysis. Arrows indicate the possible evolution direction. See also Figure S5 and Tables S1 and S3.

SIM2 in the distal small intestine could influence SIE2/3 by secreting BMP and ncWnt. The SIM11 telocytes that emerged at E13.5 secreted TGF-β, BMP, NRG, FGF, and hepatocyte growth factor (HGF).

As HGF was highly expressed in the SIM11 telocytes and might affect epithelial cells in the small intestine (Figure 5I), we explored this possibility by treating E15.5 small-intestinal organoids with HGF. HGF caused moderate morphological changes in the

CellPress
OPEN ACCESS

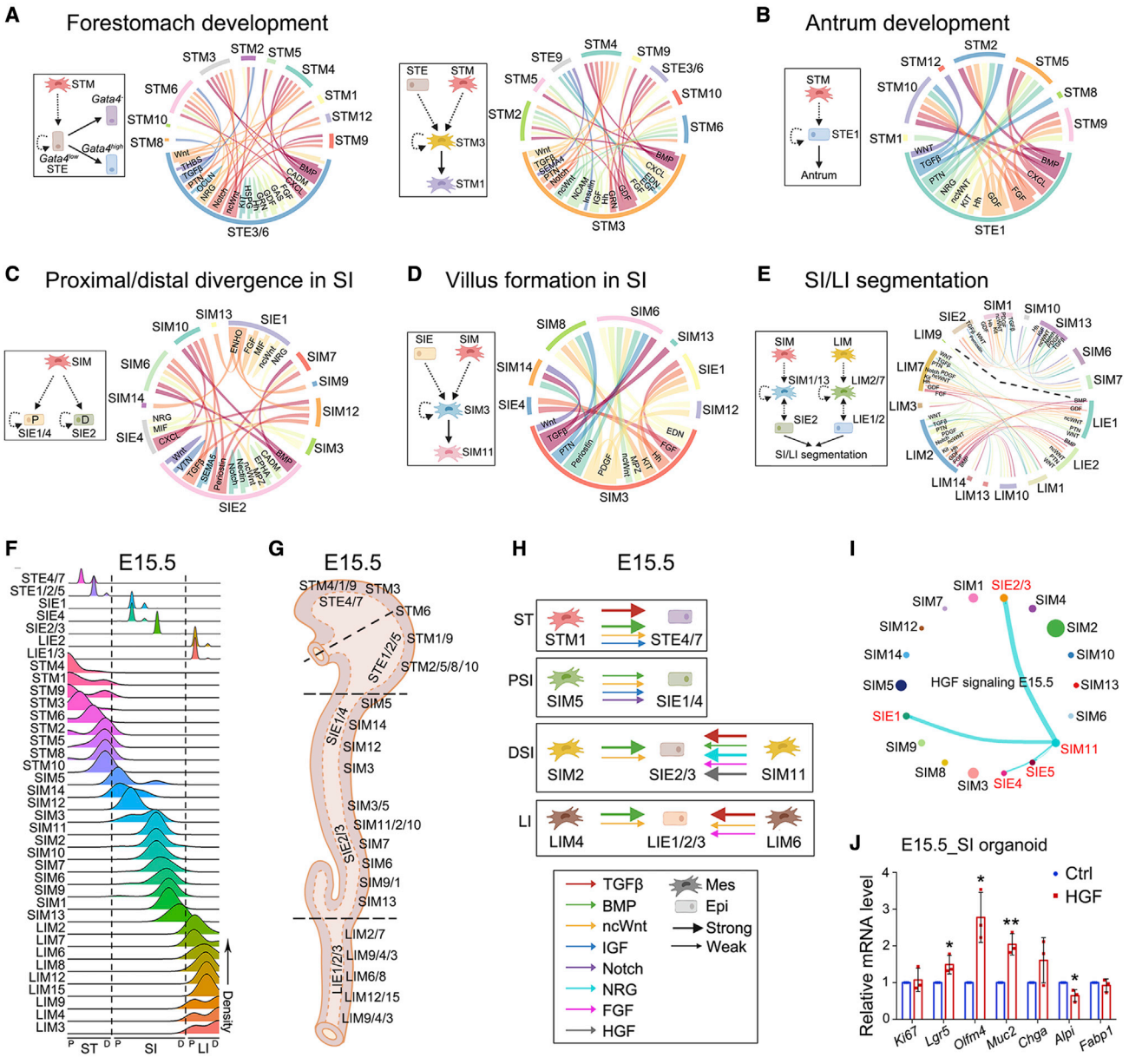

(legend on next page)

organoids (Figure S6B), but upregulated the adult stem cell marker *Olfm4*, and the secretory lineage markers *Muc2* and *Chga* were upregulated slightly (Figure 5J), implying the potential role of HGF in cell-fate determination. To further validate these results, E15.5 small intestine fragments were cultured *ex vivo* and treated with HGF. Consistently, HGF induced higher secretion of Olfm4 into the intestinal lumen (Figure 5K), although the numbers of $Muc2^+$ and $Chga^+$ epithelial cells did not obviously change (Figures S6C and S6D), possibly due to the different sensitivities of organoids and *ex vivo* tissues.

Modulation of cell fate by niche factors in gut tube-derived organoids

Organoid culture can be used to investigate the effect of the mesenchyme-derived niche factors on epithelial cell fate (Fordham et al., 2013; Holloway et al., 2021; Mustata et al., 2013; Yu et al., 2021; Zhang et al., 2020; Zhu et al., 2021). Mesenchymal-epithelial interaction analysis between E9.5 and E11.5 revealed that *Fgf10* and retinoic acid (RA) synthesis enzymes were highly expressed in the foregut or hindgut mesenchymal cells, respectively (Figure S6E). To explore the importance of niche factors in regulating early development of the GI tract, we established a culture system of organoids derived from E9.5 gut tube and tested the function of FGF10 and RA in the foregut and hindgut, respectively. As shown in Figures 6A–6C, the basic medium containing epidermal growth factor (EGF), Noggin, R-spondin1, and CHIR-99021 could support the growth of organoids derived from the foregut or hindgut, but both types of cell underwent both foregut (Sox2) and hindgut (Cdx2) fates. Importantly, FGF10 addition pushed the cell fate to the foregut, while RA together with FGF4 favored the hindgut fate. The bulk RNA-seq analysis showed that both foregut- and hindgut-derived organoids faithfully maintained their respective marker expression (Figure 6D and Table S5).

We then tested whether the niche factors could shift the cell fate by adding RA and FGF4 to the foregut organoids or FGF10 to the hindgut organoids (Figure 6A). After four passages (about 10 days), we found that the foregut-derived organoids obtained the hindgut features with RA and FGF4 and the hindgut-derived organoids gained the foregut features with FGF10, manifested by the differentially expressed marker genes Figures 6C–6F and Table S5). This result indicates that the mesenchyme-derived niche signals play a critical role to regulate epithelial cell fate determination, and also highlights the cell plasticity of the E9.5 gut tube epithelial cells.

In addition to FGF and RA signaling, there were other ligands highly expressed in specific mesenchymal cells between E9.5 and E11.5. For instance, *Bmp5*, *Dlk1*, *Rarres2*, *Postn*, *Sema5a*, and *Ncam1* are highly expressed in the intestinal mesenchyme, while *Shh* and *Kitl* are highly expressed in the intestinal epithelium (Figure S6F). To examine their possible effects on epithelial cells, we added the above ligands to the cultured hindgut-derived organoids (Figure 6G), and harvested the organoids 3 days later for bulk RNA-seq. Although the mRNA level of the typical hindgut marker *Cdx2* did not change significantly, more than 30 hindgut markers were upregulated by the addition of these factors (Figure 6H and Table S5), suggesting that these ligands could facilitate hindgut development. Therefore, these results further emphasize the important role of the mesenchyme-derived niche factors in guiding epithelium development.

DISCUSSION

In this study, we established a single-cell transcriptomic atlas of developing stomach and intestine in E9.5–E15.5. By integrating with spatial RNA-seq, we could trace the evolution process of both the epithelium and the mesenchyme in the developing GI tract, as well as their spatial interactions. Our analysis also revealed the existence of regional heterogeneity in both the epithelium and the mesenchyme at E9.5 and the critical role of the mesenchyme in regulating the regionalization and cell-fate determination of the epithelium.

The cell heterogeneity of different organs was reported at the foregut region at E8.5 (Han et al., 2020). Our data further revealed the regional cell heterogeneity in the stomach and intestine at E9.5, including the antrum regionalization in the stomach and the proximal and distal divergence in the small intestine. Moreover, the mesenchymal subpopulations also exhibited regional characteristics. Along the developmental process, more cell types could be observed, such as STE4 at E13.5 and STM1 at E11.5 in the stomach. Intriguingly, STM12 was detected only at E10.5–E13.5. These data further indicate cell heterogeneity and their dynamic evolution, which may drive the stomach morphogenesis. Similar phenomena were observed in the hindgut development. For instance, SIM1/3/9 appeared at E10.5, while SIM12 disappeared at E15.5 in the small intestine.

Figure 5. Dynamic signaling interactions between epithelial and mesenchymal cells modulate critical developmental events in stomach and intestine

(A–E) Signaling interactions drive the forestomach development (A), the antrum development (B), the divergence between proximal and distal small intestine (C), the villus formation process (D), and small and large intestine segmentation (E). Signals were analyzed by CellChat.

(F) Regional distribution of epithelial and mesenchymal subsets along the E15.5 GI tract analyzed from scRNA-seq and spatial RNA-seq. The x axis indicates location from the proximal to the distal. The y axis indicates cell density. Each row represents an individual subset of epithelial or mesenchymal cells.

(G) Map of epithelial and mesenchymal subsets along the E15.5 GI tract.

(H) Signaling events between epithelial subsets and newly formed or increased mesenchymal subsets at E13.5 and E15.5, analyzed by CellChat. PSI, proximal small intestine; DSI, distal small intestine.

(I) HGF signaling derived from SIM11 telocytes targets epithelial cells (SIEs) in the E15.5 small intestine, as revealed by CellChat analysis.

(J) Marker expression in E15.5 small-intestinal organoids treated with HGF for 5 days (two passages). Data are represented as the mean ± SD (n = 3). The statistically significant differences were calculated using an ordinary two-way ANOVA followed by Tukey's multiple comparisons test. *$p < 0.05$, **$p < 0.01$.

(K) HGF promotes Olfm4 secretion in E15.5 small intestines cultured *ex vivo*, as shown by immunofluorescence staining. The white arrow indicates secreted Olfm4 at the apical border, while the yellow arrow indicates $Olfm4^+$ cells. Longitudinal sections of cultured E15.5 small intestine were used (n = 3). Scale bars, 200 μm. See also Figure S6 and Table S4.

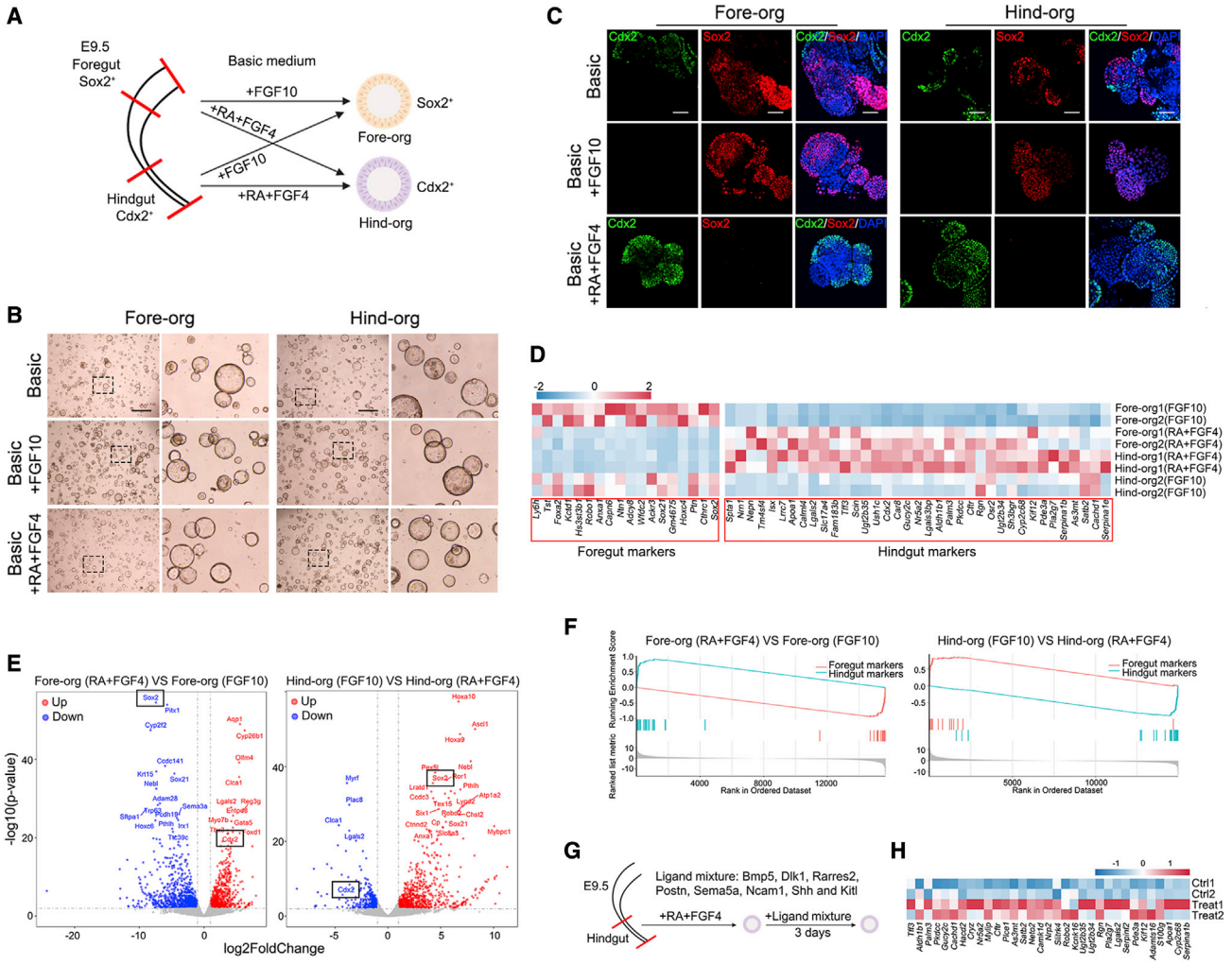

Figure 6. Modulation of cell fate by niche factors in gut tube-derived organoids

(A) Scheme of experimental design for culturing foregut- or hindgut-derived organoids. The foregut or hindgut of E9.5 gut tube was dissociated into single cells or small aggregates and then embedded into Matrigel for culture using basic medium with addition of FGF10 or RA and FGF4. After four passages, organoids were harvested for bulk RNA-seq or immunofluorescence staining. Fore-org, foregut-derived organoids; Hind-org, hindgut-derived organoids.

(B) Sphere-like organoids at P6. Scale bars, 500 μm.

(C) Expression pattern of Cdx2 and Sox2 in fore-org and hind-org under different culture media indicated by immunofluorescence staining (n = 3). Scale bars, 50 μm.

(D) Heatmap showing differentially expressed marker genes in fore-org and hind-org under different culture media, analyzed from bulk RNA-seq (n = 2).

(E) Volcano plots showing all differentially expressed genes in fore-org and hind-org under different culture media, analyzed from bulk RNA-seq.

(F) Gene-set enrichment analysis (GSEA) of differentially expressed marker genes in fore-org and hind-org under different culture media, analyzed from bulk RNA-seq.

(G and H) Ligand treatment of hindgut-derived organoids (G) for 3 days upregulates hindgut marker genes, analyzed from bulk RNA-seq and shown in the heatmap (H) (n = 2). See also Figure S6 and Table S5.

Interestingly, SIM11 highly expressed *Nrg1* and *Pdgfra*, similar to recent reported *Pdgfra*^{high}/*F3*^{high}/*Dll1*^{high} mesenchymal cells in the developing human small intestine that express NRG1 and promote epithelium differentiation (Holloway et al., 2021). The early divergence between the proximal and the distal parts may be related to the morphogenesis of different small-intestinal regions. Another recent work also showed that most cell types at E18.5 could be identified at E14.5 in the mouse large intestine (Fazilaty et al., 2021). We also observed that SIM1/13 and LIM2/7 underwent dramatic changes before E11.5 in the intestine, which may contribute to the cecum morphogenesis and small and large intestine segmentation, in line with the reported mesenchymal functions in cecum development (Zhang et al., 2006).

Lgr5, an adult stem cell marker for the intestine and gastric pylorus epithelia (Barker et al., 2007, 2010), also labels stem cell progenitors of embryonic small intestine and controls fetal intestinal stem cell maturation (Fernandez Vallone et al., 2020; Nigmatullina et al., 2017). By the *in vivo* lineage tracing experiment, we found that the *Lgr5*$^{+}$ cells should not be the stem cell progenitors before E11.5. One of the major differences between the proximal and the distal parts is the emergence of villus structure in a wave-like

formation starting from the proximal part around E14.5 (Shyer et al., 2015; Walton et al., 2012). The differential expression of *Lgr5* before villus formation raises the possibility that *Lgr5*$^{+}$ cells may play a role in epithelium morphogenesis.

The mesenchymal-epithelial interaction plays an essential role in GI tract development via the secreted niche factors (Loe et al., 2021). *Gata4*^{low} epithelial cells may drive the morphogenesis of the hindstomach (*Gata4*^{high}) and forestomach (*Gata4*$^{-}$). We found that multiple mesenchymal subsets express ncWnt, which may function in the evolution of *Gata4*^{low} epithelial cells, in line with an early report that the forestomach morphogenesis is regulated by ncWnt signaling (Matsuyama et al., 2009). We also observed that *Fgf10* is highly expressed in STM, and FGF signaling could influence both epithelial and mesenchymal evolution, consistent with its functions in stomach morphogenesis (Nyeng et al., 2007; Spencer-Dene et al., 2006). Our data also suggest that epithelium-derived signals may also regulate mesenchyme evolution. For instance, the differentiation of STM3 could be regulated by the epithelium-derived Hh signaling, which is consistent with the report that Hh signaling from epithelium could regulate stomach development by influencing mesenchyme (Mao et al., 2010). Our data suggest that SIM1/13 and LIM2/7 may be involved in the cecum morphogenesis through multiple signals, one of which is FGF signaling, in accordance with the function of FGF in the cecum formation (Al Alam et al., 2012; Zhang et al., 2006).

The role of mesenchyme in villus formation has been extensively investigated (Karlsson et al., 2000; Rao-Bhatia et al., 2020; Shyer et al., 2015; Walton et al., 2012, 2016). The mesenchyme under the epithelium could self-organize under the control of Hh and PDGF signaling, resulting in villus formation around E14.5 (Karlsson et al., 2000; Walton et al., 2012). We observed that the *Foxl1*$^{+}$/*Pdgfra*^{high} telocytes (SIM11) appear at E13.5, which may drive villus formation. This subset is also detected in the human intestine (Elmentaite et al., 2020). Our results indicate that SIM11 may be derived from SIM3, which receives Hh and PDGF signals before the emergence of SIM11, implying that the signaling guidance could occur earlier. We also found that SIM6 could modulate SIM3 via ncWnt signaling, which has been suggested to be involved in villus formation (Rao-Bhatia et al., 2020). Of note, we did not observe SIM3/11-like mesenchymal subsets in the large intestine, and it will be very interesting to know whether it accounts for lack of villus structures in the large intestine.

Limitations of this study

In this study, using scRNA-seq and spatial RNA-seq, we have dissected the cell evolution of GI epithelium and mesenchyme during E9.5–E15.5 and identified many subsets of epithelial and mesenchymal cells, but their precise distributions in the developing GI tract are still unclear. Improved high-resolution spatial RNA-seq technologies are needed (Chen et al., 2021). The role of specific subsets in GI development also needs further confirmation by depletion of these cells. Our analysis of the signaling interaction between cell subsets implicates the important functions of mesenchymal cells in regulating critical developmental events, which awaits experimental validation with genetic models. The *in vitro* and *ex vivo* results indicate that HGF could enhance the Olfm4 secretion in the developing small intestine. However, as one small-intestinal stem cell marker, the role of Olfm4 during small intestine development still needs further investigation. Although the organoid culture is a good model to investigate the role of the mesenchyme-derived niche factors, better systems are needed to mimic the *in vivo* mesenchymal-epithelial interactions. Nonetheless, our work provides a foundation for the further mechanistic illustration of GI development. As the data on human GI development are accumulating, it will be interesting to compare the developmental process and regulatory mechanisms between mouse and human.

STAR★METHODS

Detailed methods are provided in the online version of this paper and include the following:

- KEY RESOURCES TABLE
- RESOURCE AVAILABILITY
  - Lead contact
  - Materials availability
  - Data and code availability
- EXPERIMENTAL MODEL AND SUBJECT DETAILS
  - Animals
  - Organoid culture
  - *Ex vivo* culture of embryonic small intestine
- METHOD DETAILS
  - Mouse embryo dissection
  - Single-cell dissociation and single-cell RNA-seq
  - Spatial RNA-seq
  - Immunofluorescence and *in situ* hybridization
  - Bulk RNA-seq
  - qPCR analysis
- QUANTIFICATION AND STATISTICAL ANALYSIS
  - Computational analysis for scRNA-seq*Process and quality control*
  - Batch correction and unsupervised clustering
  - Differential gene expression analysis
  - Trajectory and pseudotime analysis
  - Mesenchymal-epithelial interaction analysis
  - Process and quality control of spatial RNA-seq
  - Bulk RNA-seq data analysis
  - Statistics

SUPPLEMENTAL INFORMATION

Supplemental information can be found online at https://doi.org/10.1016/j.celrep.2022.111053.

ACKNOWLEDGMENTS

We are grateful to Dr. Haiyong Zhao for help with single-cell isolation and Xu Wang for advice on RNAscope experiment. This work was supported by grants from the National Natural Science Foundation of China (31988101 and 31730056 to Y.-G.C.) and the National Key Research and Development Program of China (2017YFA0103601 to Y.-G.C.).

AUTHOR CONTRIBUTIONS

L.Z. and Y.-G.C. designed the study and analyzed the data; L.Z. performed the experiments; W.S. performed bioinformatic analyses and analyzed the data; L.Z., W.S., and Y.-G.C. wrote the manuscript.

DECLARATION OF INTERESTS

The authors declare no competing interests.

Received: January 22, 2022
Revised: March 31, 2022
Accepted: June 14, 2022
Published: July 12, 2022

REFERENCES

Al Alam, D., Sala, F.G., Baptista, S., Galzote, R., Danopoulos, S., Tiozzo, C., Gage, P., Grikscheit, T., Warburton, D., Frey, M.R., et al. (2012). FGF9-Pitx2-FGF10 signaling controls cecal formation in mice. Dev. Biol. *369*, 340–348.

Argelaguet, R., Clark, S.J., Mohammed, H., Stapel, L.C., Krueger, C., Kapourani, C.A., Imaz-Rosshandler, I., Lohoff, T., Xiang, Y., Hanna, C.W., et al. (2019). Multi-omics profiling of mouse gastrulation at single-cell resolution. Nature *576*, 487–491.

Bahar Halpern, K., Massalha, H., Zwick, R.K., Moor, A.E., Castillo-Azofeifa, D., Rozenberg, M., Farack, L., Egozi, A., Miller, D.R., Averbukh, I., et al. (2020). Lgr5+ telocytes are a signaling source at the intestinal villus tip. Nat. Commun. *11*, 1936.

Barker, N., Huch, M., Kujala, P., van de Wetering, M., Snippert, H.J., van Es, J.H., Sato, T., Stange, D.E., Begthel, H., van den Born, M., et al. (2010). Lgr5(+ve) stem cells drive self-renewal in the stomach and build long-lived gastric units in vitro. Cell Stem Cell *6*, 25–36.

Barker, N., van Es, J.H., Kuipers, J., Kujala, P., van den Born, M., Cozijnsen, M., Haegebarth, A., Korving, J., Begthel, H., Peters, P.J., et al. (2007). Identification of stem cells in small intestine and colon by marker gene Lgr5. Nature *449*, 1003–1007.

Briggs, J.A., Weinreb, C., Wagner, D.E., Megason, S., Peshkin, L., Kirschner, M.W., and Klein, A.M. (2018). The dynamics of gene expression in vertebrate embryogenesis at single-cell resolution. Science *360*.

Cao, J., Spielmann, M., Qiu, X., Huang, X., Ibrahim, D.M., Hill, A.J., Zhang, F., Mundlos, S., Christiansen, L., Steemers, F.J., et al. (2019). The single-cell transcriptional landscape of mammalian organogenesis. Nature *566*, 496–502.

Chen, A., Liao, S., Cheng, M., Ma, K., Wu, L., Lai, Y., Yang, J., Li, W., Xu, J., Hao, S., et al. (2021). Large field of view-spatially resolved transcriptomics at nanoscale resolution. Preprint at bioRxiv. https://doi.org/10.1101/2021.01.17.427004.

Chin, A.M., Hill, D.R., Aurora, M., and Spence, J.R. (2017). Morphogenesis and maturation of the embryonic and postnatal intestine. Semin. Cell Dev. Biol. *66*, 81–93.

DeLaForest, A., Kohlnhofer, B.M., Franklin, O.D., Stavniichuk, R., Thompson, C.A., Pulakanti, K., Rao, S., and Battle, M.A. (2021). GATA4 controls epithelial morphogenesis in the developing stomach to promote establishment of glandular columnar epithelium. Cell Mol. Gastroenterol. Hepatol. *S2352-345X*, 00116–00118.

Dobin, A., Davis, C.A., Schlesinger, F., Drenkow, J., Zaleski, C., Jha, S., Batut, P., Chaisson, M., and Gingeras, T.R. (2013). STAR: ultrafast universal RNA-seq aligner. Bioinformatics *29*, 15–21.

Dong, J., Hu, Y., Fan, X., Wu, X., Mao, Y., Hu, B., Guo, H., Wen, L., and Tang, F. (2018). Single-cell RNA-seq analysis unveils a prevalent epithelial/mesenchymal hybrid state during mouse organogenesis. Genome Biol. *19*, 31.

Efremova, M., Vento-Tormo, M., Teichmann, S.A., and Vento-Tormo, R. (2020). CellPhoneDB: inferring cell-cell communication from combined expression of multi-subunit ligand-receptor complexes. Nat. Protoc. *15*, 1484–1506.

Elmentaite, R., Ross, A.D.B., Roberts, K., James, K.R., Ortmann, D., Gomes, T., Nayak, K., Tuck, L., Pritchard, S., Bayraktar, O.A., et al. (2020). Single-cell sequencing of developing human gut reveals transcriptional links to childhood crohn's disease. Dev. Cell *55*, 771–783.e5.

Fazilaty, H., Brugger, M.D., Valenta, T., Szczerba, B.M., Berkova, L., Doumpas, N., Hausmann, G., Scharl, M., and Basler, K. (2021). Tracing colonic embryonic transcriptional profiles and their reactivation upon intestinal damage. Cell Rep. *36*, 109484.

Fernandez Vallone, V., Leprovots, M., Ribatallada-Soriano, D., Gerbier, R., Lefort, A., Libert, F., Vassart, G., and Garcia, M.I. (2020). LGR5 controls extracellular matrix production by stem cells in the developing intestine. EMBO Rep. *21*, e49224.

Fordham, R.P., Yui, S., Hannan, N.R., Soendergaard, C., Madgwick, A., Schweiger, P.J., Nielsen, O.H., Vallier, L., Pedersen, R.A., Nakamura, T., et al. (2013). Transplantation of expanded fetal intestinal progenitors contributes to colon regeneration after injury. Cell Stem Cell *13*, 734–744.

Gao, S., Yan, L., Wang, R., Li, J., Yong, J., Zhou, X., Wei, Y., Wu, X., Wang, X., Fan, X., et al. (2018). Tracing the temporal-spatial transcriptome landscapes of the human fetal digestive tract using single-cell RNA-sequencing. Nat. Cell Biol. *20*, 721–734.

Han, L., Chaturvedi, P., Kishimoto, K., Koike, H., Nasr, T., Iwasawa, K., Giesbrecht, K., Witcher, P.C., Eicher, A., Haines, L., et al. (2020). Single cell transcriptomics identifies a signaling network coordinating endoderm and mesoderm diversification during foregut organogenesis. Nat. Commun. *11*, 4158.

Holloway, E.M., Czerwinski, M., Tsai, Y.H., Wu, J.H., Wu, A., Childs, C.J., Walton, K.D., Sweet, C.W., Yu, Q., Glass, I., et al. (2021). Mapping development of the human intestinal niche at single-cell resolution. Cell Stem Cell *28*, 568–580.e4.

Jacobsen, C.M., Mannisto, S., Porter-Tinge, S., Genova, E., Parviainen, H., Heikinheimo, M., Adameyko, I.I., Tevosian, S.G., and Wilson, D.B. (2005). GATA-4:FOG interactions regulate gastric epithelial development in the mouse. Dev. Dyn. *234*, 355–362.

Jacobsen, C.M., Narita, N., Bielinska, M., Syder, A.J., Gordon, J.I., and Wilson, D.B. (2002). Genetic mosaic analysis reveals that GATA-4 is required for proper differentiation of mouse gastric epithelium. Dev. Biol. *241*, 34–46.

Jin, S.Q., Guerrero-Juarez, C.F., Zhang, L.H., Chang, I., Ramos, R., Kuan, C.H., Myung, P., Plikus, M.V., and Nie, Q. (2021). Inference and analysis of cell-cell communication using CellChat. Nat. Commun. *12*.

Karlsson, L., Lindahl, P., Heath, J.K., and Betsholtz, C. (2000). Abnormal gastrointestinal development in PDGF-A and PDGFR-(alpha) deficient mice implicates a novel mesenchymal structure with putative instructive properties in villus morphogenesis. Development *127*, 3457–3466.

Kim, T.H., and Shivdasani, R.A. (2016). Stomach development, stem cells and disease. Development *143*, 554–565.

Le Guen, L., Marchal, S., Faure, S., and de Santa Barbara, P. (2015). Mesenchymal-epithelial interactions during digestive tract development and epithelial stem cell regeneration. Cell. Mol. Life Sci. *72*, 3883–3896.

Loe, A.K.H., Rao-Bhatia, A., Kim, J.E., and Kim, T.H. (2021). Mesenchymal niches for digestive organ development, homeostasis, and disease. Trends Cell Biol. *31*, 152–165.

Love, M.I., Huber, W., and Anders, S. (2014). Moderated estimation of fold change and dispersion for RNA-seq data with DESeq2. Genome Biol. *15*.

Mao, J., Kim, B.M., Rajurkar, M., Shivdasani, R.A., and McMahon, A.P. (2010). Hedgehog signaling controls mesenchymal growth in the developing mammalian digestive tract. Development *137*, 1721–1729.

Matsuyama, M., Aizawa, S., and Shimono, A. (2009). Sfrp controls apicobasal polarity and oriented cell division in developing gut epithelium. PLoS Genet. *5*, e1000427.

McCracken, K.W., and Wells, J.M. (2017). Mechanisms of embryonic stomach development. Semin. Cell Dev. Biol. *66*, 36–42.

Mohammed, H., Hernando-Herraez, I., Savino, A., Scialdone, A., Macaulay, I., Mulas, C., Chandra, T., Voet, T., Dean, W., Nichols, J., et al. (2017). Single-cell landscape of transcriptional heterogeneity and cell fate decisions during mouse early gastrulation. Cell Rep. *20*, 1215–1228.

Mustata, R.C., Vasile, G., Fernandez-Vallone, V., Strollo, S., Lefort, A., Libert, F., Monteyne, D., Perez-Morga, D., Vassart, G., and Garcia, M.I. (2013). Identification of Lgr5-independent spheroid-generating progenitors of the mouse fetal intestinal epithelium. Cell Rep. *5*, 421–432.

Nichol, P.F., and Saijoh, Y. (2011). Pitx2 is a critical early regulatory gene in normal cecal development. J. Surg. Res. *170*, 107–111.

Nigmatullina, L., Norkin, M., Dzama, M.M., Messner, B., Sayols, S., and Soshnikova, N. (2017). Id2 controls specification of Lgr5(+) intestinal stem cell progenitors during gut development. EMBO J. *36*, 869–885.

Nowotschin, S., Setty, M., Kuo, Y.Y., Liu, V., Garg, V., Sharma, R., Simon, C.S., Saiz, N., Gardner, R., Boutet, S.C., et al. (2019). The emergent landscape of the mouse gut endoderm at single-cell resolution. Nature *569*, 361–367.

Nyeng, P., Norgaard, G.A., Kobberup, S., and Jensen, J. (2007). FGF10 signaling controls stomach morphogenesis. Dev. Biol. *303*, 295–310.

Peng, G., Suo, S., Cui, G., Yu, F., Wang, R., Chen, J., Chen, S., Liu, Z., Chen, G., Qian, Y., et al. (2019). Molecular architecture of lineage allocation and tissue organization in early mouse embryo. Nature *572*, 528–532.

Pijuan-Sala, B., Griffiths, J.A., Guibentif, C., Hiscock, T.W., Jawaid, W., Calero-Nieto, F.J., Mulas, C., Ibarra-Soria, X., Tyser, R.C.V., Ho, D.L.L., et al. (2019). A single-cell molecular map of mouse gastrulation and early organogenesis. Nature *566*, 490–495.

Qiu, X.J., Hill, A., Packer, J., Lin, D.J., Ma, Y.A., and Trapnell, C. (2017). Single-cell mRNA quantification and differential analysis with Census. Nat. Methods *14*, 309.

Rao-Bhatia, A., Zhu, M., Yin, W.C., Coquenlorge, S., Zhang, X., Woo, J., Sun, Y., Dean, C.H., Liu, A., Hui, C.C., et al. (2020). Hedgehog-activated Fat4 and PCP pathways mediate mesenchymal cell clustering and villus formation in gut development. Dev. Cell *52*, 647–658.e6.

Sayols, S., Klassek, J., Werner, C., Mockel, S., Ritz, S., Mendez-Lago, M., and Soshnikova, N. (2020). Signalling codes for the maintenance and lineage commitment of embryonic gastric epithelial progenitors. Development *147*, dev188839.

Shoshkes-Carmel, M., Wang, Y.J., Wangensteen, K.J., Toth, B., Kondo, A., Massassa, E.E., Itzkovitz, S., and Kaestner, K.H. (2018). Subepithelial telocytes are an important source of Wnts that supports intestinal crypts. Nature *557*, 242–246.

Shyer, A.E., Huycke, T.R., Lee, C., Mahadevan, L., and Tabin, C.J. (2015). Bending gradients: how the intestinal stem cell gets its home. Cell *161*, 569–580.

Spence, J.R., Lauf, R., and Shroyer, N.F. (2011). Vertebrate intestinal endoderm development. Dev. Dyn. *240*, 501–520.

Spencer-Dene, B., Sala, F.G., Bellusci, S., Gschmeissner, S., Stamp, G., and Dickson, C. (2006). Stomach development is dependent on fibroblast growth factor 10/fibroblast growth factor receptor 2b-mediated signaling. Gastroenterology *130*, 1233–1244.

Stuart, T., Butler, A., Hoffman, P., Hafemeister, C., Papalexi, E., Mauck, W.M., Hao, Y.H., Stoeckius, M., Smibert, P., and Satija, R. (2019). Comprehensive integration of single-cell data. Cell *177*, 1888.

Trapnell, C., Cacchiarelli, D., Grimsby, J., Pokharel, P., Li, S.Q., Morse, M., Lennon, N.J., Livak, K.J., Mikkelsen, T.S., and Rinn, J.L. (2014). The dynamics and regulators of cell fate decisions are revealed by pseudotemporal ordering of single cells. Nat. Biotechnol. *32*, 381–U251.

Walton, K.D., and Kolterud, A. (2014). Mouse fetal whole intestine culture system for ex vivo manipulation of signaling pathways and three-dimensional live imaging of villus development. J. Vis. Exp., e51817. https://doi.org/10.3791/51817.

Walton, K.D., Kolterud, A., Czerwinski, M.J., Bell, M.J., Prakash, A., Kushwaha, J., Grosse, A.S., Schnell, S., and Gumucio, D.L. (2012). Hedgehog-responsive mesenchymal clusters direct patterning and emergence of intestinal villi. Proc. Natl. Acad. Sci. U S A *109*, 15817–15822.

Walton, K.D., Whidden, M., Kolterud, A., Shoffner, S.K., Czerwinski, M.J., Kushwaha, J., Parmar, N., Chandhrasekhar, D., Freddo, A.M., Schnell, S., et al. (2016). Villification in the mouse: Bmp signals control intestinal villus patterning. Development *143*, 427–436.

Willet, S.G., and Mills, J.C. (2016). Stomach organ and cell lineage differentiation: from embryogenesis to adult homeostasis. Cell Mol. Gastroenterol. Hepatol. *2*, 546–559.

Yu, G.C., Wang, L.G., Han, Y.Y., and He, Q.Y. (2012). clusterProfiler: an R Package for comparing biological themes among gene clusters. OMICS A J. Integr. Biol. *16*, 284–287.

Yu, Q., Kilik, U., Holloway, E.M., Tsai, Y.H., Harmel, C., Wu, A., Wu, J.H., Czerwinski, M., Childs, C.J., He, Z., et al. (2021). Charting human development using a multi-endodermal organ atlas and organoid models. Cell *184*, 3281–3298.e22.

Zhang, M., Liu, Y., and Chen, Y.G. (2020). Generation of 3D human gastrointestinal organoids: principle and applications. Cell Regen. *9*, 6.

Zhang, X., Stappenbeck, T.S., White, A.C., Lavine, K.J., Gordon, J.I., and Ornitz, D.M. (2006). Reciprocal epithelial-mesenchymal FGF signaling is required for cecal development. Development *133*, 173–180.

Zhu, G., Hu, J., and Xi, R. (2021). The cellular niche for intestinal stem cells: a team effort. Cell Regen. *10*, 1.

Zorn, A.M., and Wells, J.M. (2009). Vertebrate endoderm development and organ formation. Annu. Rev. Cell Dev. Biol. *25*, 221–251.

STAR★METHODS

KEY RESOURCES TABLE

REAGENT or RESOURCE	SOURCE	IDENTIFIER
Antibodies		
Mouse monoclonal anti-Cdx2	Biogenex	Cat#MU392A-UC; RRID: AB_2650531
Rabbit monoclonal anti-Sox2	Abcam	Cat#ab92494; RRID: AB_10585428
Rabbit monoclonal anti-Rbp4	Abcam	Cat#ab188230; RRID: AB_2910554
Rabbit monoclonal anti-Clca1	Abcam	Cat#ab180851; RRID: AB_2722611
Mouse monoclonal anti-E-cadherin	BD Biosciences	Cat#610182; RRID: AB_397581
Rabbit monoclonal anti-Olfm4	Cell Signaling Technology (CST)	Cat#39141S; RRID: AB_2650511
Rabbit monoclonal anti-Muc2	Abcam	Cat#ab272692; RRID: AB_2888616
Rabbit polyclonal anti-Chga	Abcam	Cat#ab15160; RRID: AB_301704
Chemicals, peptides, and recombinant proteins		
Accutase	StemCell	Cat#07920
Collagenase I	Thermo Fisher	Cat#17100-017
DMEM/F12	Thermo Fisher	Cat#11330032
Advanced DMEM/F12	Thermo Fisher	Cat#12634028
BGJb media	Thermo Fisher	Cat#12591-038
Matrigel	BD Biosciences	Cat#356231
Penicillin/streptomycin	Thermo Fisher	Cat#15140-148
GlutaMAX	Thermo Fisher	Cat#35050-061
N2 Supplement	Thermo Fisher	Cat#17502-048
B27 Supplement	Thermo Fisher	Cat#17504-044
N-Acetylcysteine	Sigma-Aldrich	Cat#A9165
CHIR-99021	Selleck	Cat#S2924
A83-01	MedChemExpress (MCE)	Cat#HY-10432
Y27632	Selleck	Cat#S1049
Ascorbic acid	Selleck	Cat#S3114
Retinoic acid (RA)	Sigma-Aldrich	Cat#R2625
Propidium iodide (PI)	Sigma-Aldrich	Cat#P4170
DAPI	Thermo Fisher	Cat#D1306
TRIzol	Thermo Fisher	Cat#15596018
Revertra Ace	Toyobo	Cat#TRT-101
Mouse recombinant EGF	Peprotech	Cat#315-09
Mouse recombinant Noggin	Novoprotein	Cat#C028
Human recombinant R-Spondin	Novoprotein	Cat#CX83
Human recombinant FGF4	Peprotech	Cat#AF-100-31
Human recombinant FGF10	Novoprotein	Cat#CR11
Mouse recombinant HGF	Sino Biological	Cat#50038-MNAH
Human recombinant BMP5	Peprotech	Cat#120-39
Mouse recombinant RARRES2	Sino Biological	Cat#50024-M08H
Human recombinant DLK1	Novoprotein	Cat#C463
Human recombinant POSTN	Novoprotein	Cat#CJ39
Human recombinant SEMA5A	Novoprotein	Cat#C499
Human recombinant NCAM1	Novoprotein	Cat#CP45
Mouse recombinant SHH	Novoprotein	Cat#CH66

(*Continued on next page*)

Continued

REAGENT or RESOURCE	SOURCE	IDENTIFIER
Mouse recombinant KITL	Novoprotein	Cat#CB57
Critical commercial assays		
10x Chromium Single Cell 3′ GEM, Library & Gel Bead Kit v3	10X Genomics	Cat#1000075
Visium Spatial Tissue Optimization Slide & Reagents Kit	10X Genomics	Cat#1000193
Visium Spatial Gene Expression Slide & Reagents Kit	10X Genomics	Cat#1000184
RNeasy Mini Kit	Qiagen	Cat#74104
RNAscope Multiplex Fluorescent Detection Kit v2	Advanced Cell Diagnostics (ACD)	Cat#323110
Ovation RNA-Seq System V2 kit	NuGEN	Cat#7102
Deposited data		
Single cell atlas of mouse embryo stomach and intestine during E9.5-E15.5	This paper	GEO: GSE186525
Experimental models: Organisms/strains		
Mouse: *Muc2-mCherry*	This paper	N/A
Mouse: *Lgr5-CreERT2*	GemPharmatech Co. Ltd.	Cat#T003768
Mouse: *Lgr5-EGFP-IRES-CreERT2*	The Jackson Laboratory	Cat#008875
Mouse: *Rosa26-ZsGreen*	The Jackson Laboratory	Cat#007906
Oligonucleotides		
Lgr5 probe, RNAscope	Advanced Cell Diagnostics (ACD)	Cat#312171
Lox probe, RNAscope	Advanced Cell Diagnostics (ACD)	Cat#425311
Aldh1a3 probe, RNAscope	Advanced Cell Diagnostics (ACD)	Cat#501201
Adamdec1 probe, RNAscope	Advanced Cell Diagnostics (ACD)	Cat#495371
Primers for qPCR analysis	See Table S6	N/A
Software and algorithms		
R codes	This paper	https://github.com/MolcellLab/M-GI-DEV
Cellranger toolkit v4.0.0	10X Genomics	https://support.10xgenomics.com/single-cell-gene-expression/software/downloads/latest
Seurat v3.2.0	Stuart et al., 2019	https://satijalab.org/seurat
ClusterProfiler v3.16.0	Yu et al., 2012	https://bioconductor.org/packages/release/bioc/html/clusterProfiler.html
Monocle v2.16.0	Trapnell et al., 2014	https://monocle.com
CellChat v0.0.1	Jin et al., 2021	https://github.com/sqjin/CellChat
CellPhoneDB	Efremova et al., 2020	https://github.com/Teichlab/cellphonedb
Space Ranger toolkit v4.0.0	10X Genomics	https://support.10xgenomics.com/spatial-gene-expression/software/downloads/latest
STAR	Dobin et al., 2013	http://code.google.com/p/rna-star/
DESeq2 v1.28.1	Love et al., 2014	https://bioconductor.org/packages/release/bioc/html/DESeq2.html
Photoshop CC 2017	Adobe	https://www.adobe.com/products/photoshop
Prism v9	Graphpad	https://www.graphpad.com/scientificsoftware/prism/

(*Continued on next page*)

Continued

REAGENT or RESOURCE	SOURCE	IDENTIFIER
Other		
Tungsten needles	FST	10130–10
Dumont forceps	FST	11252–00

RESOURCE AVAILABILITY

Lead contact

Further information and requests for resources and reagents should be directed to and will be fulfilled by the lead contact, Ye-Guang Chen (ygchen@tsinghua.edu.cn).

Materials availability

This study did not generate new unique reagents.

Data and code availability

- Single-cell and bulk RNA-seq data have been deposited at GEO and are publicly available as of the date of publication. Accession numbers are listed in the key resources table. Microscopy data reported in this paper will be shared by the lead contact upon request.
- All original code has been deposited at GitHub and is publicly available as of the date of publication. DOIs are listed in the key resources table.
- Any additional information required to reanalyze the data reported in this paper is available from the lead contact upon request.

EXPERIMENTAL MODEL AND SUBJECT DETAILS

Animals

Muc2-mCherry mice were generated in our laboratory. *Lgr5-CreERT2* mice (T003768) were obtained from GemPharmatech Co. Ltd. *Lgr5-EGFP-IRES-CreERT2* mice (#008875) and *Rosa26-ZsGreen* mice (#007906) were obtained from the Jackson Laboratory. Natural mating was set up between 2 and 3 months old males and 2-3 months old virgin females, with noon of the day of vaginal plug considered to be E0.5. Single cells for RNA-seq were derived from C57BL/6 wild-type embryos at E9.5, E10.5, E11.5, E13.5 and E15.5 stages. Tissue sections for spatial RNA-seq were obtained from C57BL/6 wild-type embryos at E13.5 and E15.5 stages. For the detection of *Muc2* expression, tissue sections from *Muc2-mCherry* embryos at E14.5 and E15.5 stages were used. For the detection of *Lgr5* expression, tissue sections from *Lgr5-CreERT2; Rosa26-ZsGreen* and *Lgr5-EGFP-IRES-CreERT2* embryos at E15.5 stage were used. All embryonic experiments included both sexes. All mice were housed in the pathogen-free Laboratory Animal Facility of Tsinghua University under a 12-h light/dark cycle. All animal studies were performed in accordance with the relevant guidelines and under the approval of the Institutional Animal Care and Use Committee of Tsinghua University.

Organoid culture

Embryonic tissues for organoid culture were isolated at E9.5 (gut tube) or E15.5 (small intestine) stages. E9.5 gut tubes were divided into foregut and hindgut parts (connection part excluded) and then dissociated into single cells or small aggregates in Accutase (StemCell) under 37°C for 5 min. Cells were embedded into Matrigel (BD Biosciences) after centrifugation (3 min at 1000 rpm). After polymerization, the basic medium plus FGF10 (100 ng/mL, Novoprotein) or RA (2 μM, Sigma) and FGF4 (500 ng/mL, Peprotech) were added. Two days later, organoids were passaged every day to remove the growing mesenchymal cells.

The culture of E15.5 small intestinal organoids was modified from published work (Mustata et al., 2013). Briefly, E15.5 small intestines were dissected and cut into pieces, then dissociated in 0.2% collagenase I (17100-017, Thermo Fisher) in DMEM/F12 under 37°C for 30 min (pipette every 5 min) and subsequent Accutase under 37°C for 15 min (pipette every 5 min). Cells were embedded into Matrigel (BD Biosciences) after centrifugation (3 min at 1000 rpm). After polymerization, the basic medium was added. After several passages, HGF (500 ng/mL, Sino Biological) was added into the basic medium and stimulated for 5 days (2 passages).

The basic medium (Advanced DMEM/F12, Thermo Fisher) consists of penicillin/streptomycin (Thermo Fisher), GlutaMAX (Thermo Fisher), N2 (Thermo Fisher), B27 (Thermo Fisher), N-acetylcysteine (Sigma-Aldrich), EGF (50 ng/mL, Peprotech), Noggin (100 ng/mL, Novoprotein), R-spondin1 (500 ng/mL, Novoprotein), CHIR-99021 (5 μM, Selleck), A83-01 (5 nM, MCE), and Y27632 (100 nM, Selleck). The following ligands were used in stimulation experiments: Bmp5 (50 ng/mL, Peprotech), Rarres2 (500 ng/mL, Sino Biological), Dlk1 (500 ng/mL, Novoprotein), Postn (500 ng/mL, Novoprotein), Sema5a (500 ng/mL, Novoprotein), Ncam1 (500 ng/mL, Novoprotein), Shh (500 ng/mL, Novoprotein), Kitl (500 ng/mL, Novoprotein).

Ex vivo culture of embryonic small intestine

Embryonic small intestines were isolated at E15.5 stage. *Ex vivo* culture of embryonic small intestine was performed as reported (Walton and Kolterud, 2014). Briefly, pieces of E15.5 small intestines (2.5–4.0 mm long) were dissected from embryos. After separating connective tissues, the intestines were placed on transwells (3428, Corning) and cultured in BGJb media (12591-038, Thermo Fisher) supplemented with penicillin/streptomycin (Thermo Fisher) and 0.1 mg/mL ascorbic acid (Selleck). Intestines were cultured for 3 days with Hgf (500 ng/mL, Sino Biological) or not at 37°C with 5% CO2 with media changes every 24 h.

METHOD DETAILS

Mouse embryo dissection

Isolated embryos were kept and dissected in DMEM/F12 (Corning), containing 10% fetal calf serum (Hyclone). Digestive tracts were carefully dissected under stereomicroscope using tungsten needles (10130-10, FST) and Dumont forceps (11252-00, FST). To capture more precise spatial information, the digestive tracts were dissected into individual sampling parts for sequencing based on tissue morphologies. Since the boundary between foregut and mid/hindgut at E9.5 is not clear enough for segmentation, the whole gut tube of this stage was taken as one sample. The E10.5 gut tube was separated into stomach and intestine, while the individual stomach, small intestine and large intestine were included in the E11.5, E13.5 and E15.5 samples, the small intestine at E13.5 and E15.5 was further separated into proximal and distal part. For E11.5-E15.5 samples, the cecum part was excluded. We pooled 12, 8, 8, 6, 6 embryonic GI samples for E9.5, E10.5, E11.5, E13.5 and E15.5, respectively, for scRNA-seq.

Single-cell dissociation and single-cell RNA-seq

For E9.5-E13.5 samples, different parts were cut into small pieces and dissociated in Accutase under 37°C for 5 min (E9.5), 10 min (E10.5), 15 min (E11.5) and 30 min (E13.5) with gently pipetting up and down every 5 min. For E15.5 samples, different parts were cut into small pieces and dissociated in 0.2% collagenase I (17100-017, Thermo Fisher) in DMEM/F12 under 37°C for 30 min (pipette every 5 min) and then in Accutase under 37°C for 15 min (pipette every 5 min). After dissociation, the cell suspension was stained by propidium iodide (PI, 5 μg/mL) and sorted for PI-negative single cells by FACS (BeckMan). Then single cells were captured in the 10X Genomics Chromium Single Cell 3′ Solution, and RNA-seq libraries were generated following the manufacturer's instruction (10X Genomics) and subjected to high-throughput sequencing on an Illumina Novaseq PE150 platform.

Spatial RNA-seq

Tissues were quickly embedded in optimal cutting temperature compound (OCT) on dry ice and then stored in −80°C no more than 1 month. Before undergoing the formal spatial RNA-seq protocol, several frozen sections were subjected to RNA extraction (74104, Qiagen) and RNA quality test with RIN>7.0 for standard (Agilent). To get optimized time for tissue permeabilization, the tissue optimization experiment (1000193, 10X Genomics) was performed and the fluorescence was captured by microscopy (Nikon), determining 3 min as tissue permeabilization time. For formal spatial RNA-seq experiment, 10 μm frozen sections were cut (Leica) onto capture regions within 10X Visium slides, and then spatial RNA-seq was performed following the manufacturer's instruction (1000184, 10X Genomics). The images of H&E staining were captured (KEYENCE), and the libraries were subjected to high-throughput sequencing on an Illumina Novaseq PE150 platform.

Immunofluorescence and *in situ* hybridization

For immunofluorescence of tissue sections, the gut tube tissues were washed in cold PBS, fixed with 4% formaldehyde for 30 min (overnight at 4°C for *ex vivo* culture tissues) and dehydrated in 30% sucrose for at least 5 h with shaking at room temperature (12 h for *ex vivo* culture tissues). Next, the tissues were embedded with OCT and frozen at −80°C before cut (Leica) to 10 μm thickness. Before staining, sections were dried for 15 min at room temperature, then put into PBS for 5 min to remove OCT. The sections underwent antigen retrieval in 95°C water bath for 25 min, then were permeabilized with 0.1% Triton X-100 for 15 min at 4°C, followed by blocked with 3% BSA and 0.01% Triton X-100 for 1 h at room temperature. Next, the sections were incubated with primary antibodies at 4°C overnight before the fluorescein-labeled secondary antibodies (1:300, Life Technologies) with DAPI (Thermo Fisher) were added for 1 h at room temperature.

For immunofluorescence of organoids, the organoids were resuspended in PBS and washed, then fixed with 4% formaldehyde for 15 min with shaking at room temperature. The organoids were permeabilized with 0.2% Triton X-100 for 20 min with shaking at 4°C, followed by blocked with 1% BSA for 1 h with shaking at room temperature. Next, the organoids were incubated with primary antibodies at 4°C with shaking overnight before the fluorescein-labeled secondary antibodies (1:300, Life Technologies) with DAPI were added for 1 h with shaking at room temperature. Then the organoids were placed on glass slides and covered. The images were captured by Confocal laser scanning (FV3000, Olympus). The following primary antibodies were used: mouse anti-Cdx2 (1:100, MU392A-UC; Biogenex); rabbit anti-Sox2 (1:200, ab92494; Abcam); rabbit anti-Rbp4 (1:100, ab188230; Abcam); rabbit anti-Clca1 (1:100, ab180851; Abcam); mouse anti-E-cadherin (1:500, 610182; BD Biosciences); rabbit anti-Olfm4 (1:200, 39141S; CST); rabbit anti-Muc2 (1:200, ab272692; Abcam) and rabbit anti-Chga (1:200, ab15160; Abcam).

For *in situ* hybridization (RNAscope) of tissue sections, fresh tissues were quickly embedded in OCT on dry ice and then stored in −80°C no more than 1 week. Frozen sections were cut (Leica) to 10 μm thickness and stored at −80°C overnight. The sections were

fixed in 10% neutral buffered formalin (Solarbio) for 15 min at 4°C, followed by dehydrated in graded ethanol. Endogenous peroxidase blocking was performed by hydrogen peroxide (322381, ACD) for 10 min at room temperature. Then, Protease III (322381, ACD) was added for 20 min at room temperature before probe hybridization. Probes (Lgr5, 312171, ACD; Lox, 425311, ACD; Aldh1a3, 501201, ACD; Adamdec1, 495371, ACD) were used for 2 h at 40°C, AMP 1-3, and signal detection was performed as described in the user manual (323110, ACD). The images were captured by Confocal laser scanning (FV3000, Olympus).

Bulk RNA-seq

The organoids were subjected to RNA extraction (74104, Qiagen). cDNA libraries were conducted using the Ovation RNA-Seq System V2 kit (NuGEN) and then subjected to high-throughput sequencing on an Illumina Novaseq PE150 platform. RNA-seq was carried out with two biological replicates.

qPCR analysis

Total RNA from organoids was extracted using TRIzol (Thermo Fisher). cDNA was prepared using Revertra Ace (Toyobo). qPCR was performed in triplicates on a LightCycler 480 (Roche) with GAPDH as the reference gene. Data were analyzed according to the ΔCT method. The primer sequences were listed in Table S6.

QUANTIFICATION AND STATISTICAL ANALYSIS

Computational analysis for scRNA-seq*Process and quality control*

The raw sequencing reads were first demultiplexed using Illumina bcl2fastq software to generate 150-bp paired-end read files in FASTQ format. The reads were then aligned to the mm10 mouse reference genome using the Cellranger toolkit (v4.0.0) provided by 10X Genomics. The exonic reads uniquely mapped to the transcriptome were then used for unique molecular identifier (UMI) counting. After selection and filtering of the droplet barcodes, the filtered single cells and their UMI count matrices were imported into R package Seurat for further analysis. After discarding the genes expressed in fewer than three cells, and cells with genes less than 200, low-quality cells were filtered. Moreover, cells with more than 10 percent of mitochondrial genes expression were also discarded.

Batch correction and unsupervised clustering

Data normalization was performed using Seurat NormalizeData. Single-cell RNA-seq data of different segments from 5 time points were integrated into one object using Seurat (v3.2.0) (Stuart et al., 2019). In brief, features anchored each sample pairs were calculated using FindIntefrationAnchors function, all 14 batches of data were pooled into a single object for subsequent analyses based on anchors using IntegrateData. To regress out impression of cell cycle stage of each cell, cell cycle annotation was performed using the CellCycleScoring function in Seurat, which assigns each cell a score based on the expression of 43 marker genes for the G2/M phase and 54 marker genes for the S phase. Then graph-based clustering was performed, which allocated cells in a K-nearest neighbor graph structure, and each cell was iteratively clustered. Finally, we used uniform manifold approximation and projection for dimension reduction (UMAP) to place cells with similar local neighborhoods in high-dimensional space or low-dimensional space based on scaled expression of variable genes to visualize the clustering results of all the cells.

Differential gene expression analysis

To identify signature genes of each cell type, the functions FindAllMarkers and FindMarkers in Seurat were used with default parameter. For a given cluster, FindAllMarkers-identified positive markers were compared with all other cells using 'wilcox'. All the detailed results of differentially expressed genes were listed in supplementary Supplementary Tables. Expression heatmaps of the signature genes for each cluster are shown in corresponding Figures. Similarly, the function FindMarkers was used for identification of signature genes by comparing cluster pairs of interest. GO (Gene Ontology) and KEGG (Kyoto Encyclopedia of Genes and Genomes) enrichment analyses of significant genes were performed by R package ClusterProfiler (Yu et al., 2012).

Trajectory and pseudotime analysis

Cell trajectories of epithelial and mesenchymal cells of stomach, small intestine and large intestine at different time points were inferred using the R package Monocle (v2.16.0) (Trapnell et al., 2014). Raw single cell gene expression data were loading to create new monocle object and then normalized based on SizeFactors. Data dimension was reduced using the DDRTree method by reduceDimension based on highly dispersion genes expression. Cells were ordered along the trajectory using orderCells. UMAP plots of epithelial and mesenchymal cells of the stomach, small intestine and large intestine were colored by pseudotime calculated by Monocle. Genes essential to cell fate decision with branch-dependent expression were identified using BEAM (Qiu et al., 2017).

Mesenchymal-epithelial interaction analysis

Interactions of different mesenchymal-epithelial cells types in each segment from five time points were inferred using CellChat (v0.0.1) (Jin et al., 2021) and CellPhoneDB (Efremova et al., 2020). Ligands, receptors and their cofactors interaction data of each signaling pathways were provided by CellChatDB (Table S4). Normalized gene expression matrix of each cell and cell-cluster

meta data of corresponding Seurat objects were used to construct CellChat objects. Major signaling inputs and outputs for each cluster and their contribution scores were calculated by the identifyCommunicationPatterns function based on the expression level of ligands and receptors of single cells. Major signaling sources and targets, as well as mediators and influencers were also measured from network analysis of CellChat. Moreover, cell-cell communication mediated by ligand-receptor complexes were calculated using CellPhoneDB. Normalized gene expression matrix of subclusters with more than 10 cells from the stomach, small intestine and large intestine at five points were used as input, separately. Mean values of significant ligand-receptors pairs filtered by default significance cutoff of each segment at each time point were merged, and key signaling related pairs were shown in heatmap.

Process and quality control of spatial RNA-seq

The raw sequencing reads of spatial RNA-seq were aligned to the mm10 mouse reference genome using the Space Ranger toolkit (v4.0.0) of 10X Genomics. Spots-UMI count matrices and corresponding spatial image of E13.5 and E15.5 samples were then loading to Seurat object. Moreover, segment parts and mesenchymal epithelial site of each spot were manually annotated. The SCTransform function of Seurat was used to normalize, scale gene expression and regress out effect by both mitochondrial gene expression percentage and cell cycle stage of each cell. The TransferData function of Seurat was performed to combine cluster information from single cell RNA-seq data and spatial information from spatial RNA-seq data. Corresponding clusters of each spot were predicted using single cell RNA-seq data as anchor set, each spot was marked by corresponding cluster with max sore. Spatial sites for each cell of single cell RNA-seq were predicted using spatial data as anchor sets.

Bulk RNA-seq data analysis

For bulk RNA-seq data of organoids, sequencing reads were aligned to mm10 mouse genome reference (GRCh38) using STAR (Spliced Transcripts Alignment to a Reference) with default parameter (Dobin et al., 2013). The R package DESeq2 (Love et al., 2014) was then used to perform differential expression analysis using gene counts data calculated by STAR. Differential expressed genes with Log2FoldChange absolute value > 1 and p value <0.01 were used to do GO and KEGG enrichment analysis using R package ClusterProfiler. GSEA (Gene Set Enrichment Analysis) of featured genes of the foregut and hindgut were also performed by ClusterProfiler.

Statistics

Images were prepared using Adobe Photoshop CC (2017). Statistical analyses were performed using Prism (v9). The statistically significant differences were calculated using an ordinary two-way ANOVA followed by Tukey's multiple comparisons test. n.s: not significant, *: p value < 0.05, **: p value <0.01.